## References


[1] Y.M. Ayala, T. Misteli, F.E. Baralle, TDP-43 regulates retinoblastoma protein phosphorylation through the repression of cyclin-dependent kinase 6 expression, Proc. Natl. Acad. Sci. U.S.A. 105 (2008) 3785–3789.

[2] Y.M. Ayala, F. Pagani, F.E. Baralle, TDP43 depletion rescues aberrant CFTR exon 9 skipping, FEBS Lett. 580 (2006) 1339–1344.

[3] E. Buratti, F.E. Baralle, Multiple roles of TDP-43 in gene expression, splicing regulation, and human disease, Front. Biosci. 13 (2008) 867–878.

[4] S.H. Ou, F. Wu, D. Harrich, et al., Cloning and characterization of a novel cellular protein, TDP-43, that binds to human immunodeficiency virus type 1 TAR DNA sequence motifs, J. Virol. 69 (1995) 3584–3596.

[5] I.F. Wang, N.M. Reddy, C.K. Shen, Higher order arrangement of the eukaryotic nuclear bodies, Proc. Natl. Acad. Sci. U.S.A. 99 (2002) 13583–13588.

[6] T. Arai, M. Hasegawa, H. Akiyama, et al., TDP-43 is a component of ubiquitin-positive tau-negative inclusions in frontotemporal lobar degeneration and amyotrophic lateral sclerosis, Biochem. Biophys. Res. Commun. 351 (2006) 602–611.

[7] M. Neumann, D.M. Sampathu, L.K. Kwong, et al., Ubiquitinated TDP-43 in frontotemporal lobar degeneration and amyotrophic lateral sclerosis, Science 314 (2006) 130–133.

[8] T. Arai, I.R. Mackenzie, M. Hasegawa, et al., Phosphorylated TDP-43 in Alzheimer's disease and dementia with Lewy bodies, Acta Neuropathol. (Berl) 117 (2009) 125–136.

[9] M. Hasegawa, T. Arai, H. Akiyama, et al., TDP-43 is deposited in the Guam parkinsonism-dementia complex brains, Brain 130 (2007) 1386–1394.

[10] C.F. Tan, M. Yamada, Y. Toyoshima, et al., Selective occurrence of TDP-43-immunoreactive inclusions in the lower motor neurons in Machado-Joseph disease, Acta Neuropathol. (Berl) 118 (2009) 553–560.

[11] Y. Toyoshima, H. Tanaka, M. Shimohata, et al., Spinocerebellar ataxia type 2 (SCA2) is associated with TDP-43 pathology, Acta Neuropathol. (Berl) 122 (2011) 375–378.

[12] O. Yokota, Y. Davidson, E.H. Bigio, et al., Phosphorylated TDP-43 pathology and hippocampal sclerosis in progressive supranuclear palsy, Acta Neuropathol. (Berl) 120 (2010) 55–66.

[13] E. Kabashi, P.N. Valdmanis, P. Dion, et al., TARDBP mutations in individuals with sporadic and familial amyotrophic lateral sclerosis, Nat. Genet. 40 (2008) 572–574.

[14] J. Sreedharan, I.P. Blair, V.B. Tripathi, et al., TDP-43 mutations in familial and sporadic amyotrophic lateral sclerosis, Science 319 (2008) 1668–1672.

[15] A. Tamaoka, M. Arai, M. Itokawa, et al., TDP-43 M337V mutation in familial amyotrophic lateral sclerosis in Japan, Intern. Med. 49 (2010) 331–334.

[16] I.R. Mackenzie, R. Rademakers, M. Neumann, TDP-43 and FUS in amyotrophic lateral sclerosis and frontotemporal dementia, Lancet Neurol. 9 (2010) 995–1007.

[17] M. Hasegawa, T. Arai, T. Nonaka, et al., Phosphorylated TDP-43 in frontotemporal lobar degeneration and amyotrophic lateral sclerosis, Ann. Neurol. 64 (2008) 60–70.

[18] I.R. Mackenzie, E.H. Bigio, P.G. Ince, et al., Pathological TDP-43 distinguishes sporadic amyotrophic lateral sclerosis from amyotrophic lateral sclerosis with SOD1 mutations, Ann. Neurol. 61 (2007) 427–434.

[19] M. Neumann, L.K. Kwong, A.C. Truax, et al., TDP-43-positive white matter pathology in frontotemporal lobar degeneration with ubiquitin-positive inclusions, J. Neuropathol. Exp. Neurol. 66 (2007) 177–183.

[20] H. Zhang, C.F. Tan, F. Mori, et al., TDP-43-immunoreactive neuronal and glial inclusions in the neostriatum in amyotrophic lateral sclerosis with and without dementia, Acta Neuropathol. (Berl) 115 (2008) 115–122.

[21] M. Neumann, I.R. Mackenzie, N.J. Cairns, et al., TDP-43 in the ubiquitin pathology of frontotemporal dementia with VCP gene mutations, J. Neuropathol. Exp. Neurol. 66 (2007) 152–157.

[22] H.X. Zhang, K. Tanji, F. Mori, et al., Epitope mapping of 2E2-D3, a monoclonal antibody directed against human TDP-43, Neurosci. Lett. 434 (2008) 170–174.

[23] T. Nonaka, F. Kametani, T. Arai, et al., Truncation and pathogenic mutations facilitate the formation of intracellular aggregates of TDP-43, Hum. Mol. Genet. 18 (2009) 3353–3364.

[24] T. Nonaka, T. Arai, E. Buratti, et al., Phosphorylated and ubiquitinated TDP-43 pathological inclusions in ALS and FTLD-U are recapitulated in SH-SY5Y cells, FEBS Lett. 583 (2009) 394–400.

[25] Y. Nishimoto, D. Ito, T. Yagi, et al., Characterization of alternative isoforms and inclusion body of the TAR DNA-binding protein-43, J. Biol. Chem. 285 (2010) 608–619.

[26] E. Buratti, F.E. Baralle, Characterization and functional implications of the RNA binding properties of nuclear factor TDP-43, a novel splicing regulator of CFTR exon 9, J. Biol. Chem. 276 (2001) 36337–36343.

[27] H. Wils, G. Kleinberger, J. Janssens, et al., TDP-43 transgenic mice develop spastic paralysis and neuronal inclusions characteristic of ALS and frontotemporal lobar degeneration, Proc. Natl. Acad. Sci. U.S.A. 107 (2010) 3858–3863.

[28] L.M. Igaz, L.K. Kwong, A. Chen-Plotkin, et al., Expression of TDP-43 C-terminal Fragments in Vitro Recapitulates Pathological Features of TDP-43 Proteinopathies, J. Biol. Chem. 284 (2009) 8516–8524.

[29] M. Hasegawa, T. Nonaka, H. Tsuji, et al., Molecular Dissection of TDP-43 Proteinopathies, J. Mol. Neurosci. 45 (2011) 480–485.

[30] J. Collinge, K.C. Sidle, J. Meads, et al., Molecular analysis of prion strain variation and the aetiology of 'new variant' CJD, Nature 383 (1996) 685–690.

[31] H. Miake, H. Mizusawa, T. Iwatsubo, et al., Biochemical characterization of the core structure of alpha-synuclein filaments, J. Biol. Chem. 277 (2002) 19213–19219.

[32] M. Novak, J. Kabat, C.M. Wischik, Molecular characterization of the minimal protease resistant tau unit of the Alzheimer's disease paired helical filament, EMBO J. 12 (1993) 365–370.

J Mol Neurosci
DOI 10.1007/s12031-011-9571-x

# Molecular Dissection of TDP-43 Proteinopathies

**Masato Hasegawa · Takashi Nonaka · Hiroshi Tsuji · Akira Tamaoka · Makiko Yamashita · Fuyuki Kametani · Mari Yoshida · Tetsuaki Arai · Haruhiko Akiyama**

Received: 30 April 2011 / Accepted: 2 June 2011


**Abstract** TDP-43 has been identified as a major component of ubiquitin-positive tau-negative cytoplasmic inclusions in frontotemporal lobar degeneration with ubiquitin-positive inclusions (FTLD-U) and in amyotrophic lateral sclerosis (ALS). We raised antibodies to phosphopeptides representing 36 out of 64 candidate phosphorylation sites of human TDP-43 and showed that the antibodies to pS379, pS403/404, pS409, pS410 and pS409/410 labeled the inclusions, but not the nuclei. Immunoblot analyses demonstrated that the antibodies recognized TDP-43 at ~45 kDa, smearing substances and 18–26 kDa C-terminal fragments. Furthermore, the band patterns of the C-terminal fragments differed between neuropathological subtypes, but were indistinguishable between brain regions and spinal cord in each individual patient. Protease treatment of Sarkosyl-insoluble TDP-43 suggests that the different band patterns of the C-terminal fragments reflect different conformations of abnormal TDP-43 molecules between the diseases. These results suggest that molecular species of abnormal TDP-43 are different between the diseases and that they propagate from affected cells to other cells during disease progression and determine the clinicopathological phenotypes of the diseases.

**Keywords** Propagation · Phosphorylation · Tau · α-Synuclein · Prion · Cancer

M. Hasegawa (✉) · T. Nonaka · H. Tsuji · M. Yamashita · F. Kametani
Department of Neuropathology and Cell Biology,
Tokyo Metropolitan Institute of Medical Science,
2-1-6 Kamikitazawa, Setagaya-ku,
Tokyo 156–8506, Japan
e-mail: hasegawa-ms@igakuken.or.jp

M. Hasegawa · T. Nonaka · M. Yamashita · F. Kametani · T. Arai · H. Akiyama
Dementia Research Project,
Tokyo Metropolitan Institute of Medical Science,
2-1-6 Kamikitazawa, Setagaya-ku,
Tokyo 156–8506, Japan

H. Tsuji · A. Tamaoka
Department of Neurology, Graduate School of Comprehensive Human Sciences, University of Tsukuba,
Ibaraki 305–8577, Japan

M. Yoshida
Department of Neuropathology,
Institute for Medical Science of Aging, Aichi Medical University,
21 Karimata, Yazako, Nagakute-cho, Aichi-gun,
Aichi 480–1195, Japan

T. Arai
Department of Psychiatry, Graduate School of Comprehensive Human Sciences, University of Tsukuba,
Ibaraki 305–8577, Japan

## Introduction

TAR DNA-binding protein of $M_r$=43 kDa (TDP-43) is a nuclear factor that functions in regulating transcription and splicing. It is structurally characterized by two RNA recognition motifs and the C-terminal tail containing a glycine-rich region, and resembles a heterogeneous ribonucleoprotein (hnRNP) (Ayala et al. 2005). It has been shown to interact with several nuclear ribonucleoproteins (RNP), including hnRNP A and B and survival motor neuron protein, inhibiting alternative splicing (Buratti et al. 2005; Bose et al. 2008). In 2006, TDP-43 was identified as a major component of ubiquitin-positive inclusions in frontotemporal lobar degeneration with ubiquitin-positive inclusions (FTLD-U) and amyotrophic lateral sclerosis (ALS) (Arai et al. 2006; Neumann et al. 2006). Subsequent immunohistochemical examination demonstrated abnormal accumulation of TDP-43 in neurodegenerative disorders other than FTLD-U and ALS, including ALS/parkinsonism–

Published online: 16 June 2011

dementia complex of Guam (Geser et al. 2007; Hasegawa et al. 2007), Alzheimer's disease (AD) (Amador-Ortiz et al. 2007; Higashi et al. 2007; Arai et al. 2009), dementia with Lewy bodies (DLB) (Higashi et al. 2007; Nakashima-Yasuda et al. 2007; Arai et al. 2009), Pick's disease (Arai et al. 2006; Freeman et al. 2008; Lin and Dickson 2008), argyrophilic grain disease (Fujishiro et al. 2009) and corticobasal degeneration (Uryu et al. 2008). These diseases with TDP-43 pathologies are now referred to as TDP-43 proteinopathies. In 2008, mutations in the TDP-43 gene (*TARDBP*) were discovered in familial and sporadic cases of ALS (Yokoseki et al. 2008; Gitcho et al. 2008; Sreedharan et al. 2008; Kabashi et al. 2008; Van Deerlin et al. 2008; Barmada and Finkbeiner 2010; Pesiridis et al. 2009), FTD-MND (Benajiba et al. 2009) and FTD (Borroni et al. 2009), clearly indicating that abnormality of TDP-43 protein causes neurodegeneration.

## Identification of Abnormal Phosphorylation Sites of TDP-43

Biochemical analyses of the detergent-insoluble fraction extracted from brains of patients afflicted with FTLD-TDP and ALS show that TDP-43 accumulated in these pathological structures is phosphorylated and cleaved (Arai et al. 2006; Neumann et al. 2006). By producing antibodies against synthetic phosphopeptides containing 36 different phosphorylation sites from among the 56 serine/threonine residues of TDP-43, five abnormal phosphorylation sites were identified at serine residues in the C-terminal region (Hasegawa et al. 2008). The antibodies to pS379, pS403/404, pS409, pS410 and pS409/410 strongly stain abnormal neuronal cytoplasmic and dendritic inclusions in FTLD-U, and skein-like and glial cytoplasmic inclusions in ALS spinal cord, with no nuclear staining, and thus permit easier and more sensitive detection of abnormal TDP-43 accumulation in neuropathological examinations (Hasegawa et al. 2008). Immunoblotting of the Sarkosyl-insoluble fraction from control, FTLD-U and ALS cases using these phospho-specific antibodies clearly demonstrated that hyperphosphorylated full-length TDP-43 at ~45 kDa, smearing substances and fragments at 18–26 kDa are the major species of TDP-43 accumulated in FTLD-U and ALS (Hasegawa et al. 2008).

## Cellular Models of TDP-43

To establish cellular models of TDP-43 proteinopathies, several deletion mutants of human TDP-43 in SH-SY5Y cells were expressed and the accumulation of TDP-43 was analyzed by use of the phospho-TDP-43 antibodies and ubiquitin. Wild-type (WT) full-length TDP-43 was localized to nuclei and no inclusions were observed, whereas in cells transfected with C-terminal fragments as GFP fusions, round cytoplasmic inclusions with intense GFP fluorescence were formed (Nonaka et al. 2009b). In addition, a deletion mutant lacking the nuclear localizing signal (NLS) and six amino acids similar to the NLS also formed aggregates in cells without any treatment (Nonaka et al. 2009a). These inclusions are strongly positive for antibodies to phosphorylated TDP-43 and ubiquitin. Using these cellular models, the effect of pathogenic mutations of the TDP-43 gene was analyzed. Of 14 mutants examined, seven mutants showed a significantly higher number of aggregates than the WT C-terminal fragment, strongly suggesting that these mutations of TDP-43 accelerate aggregation of the C-terminal fragments (Nonaka et al. 2009b). In addition, when GFP-tagged C-terminal fragments were co-expressed with DsRed-tagged full-length TDP-43, cytoplasmic inclusions with both GFP and DsRed signals were formed, suggesting that exogenous full-length TDP-43 is trapped in cytoplasmic inclusions formed by C-terminal fragments. This may explain why normal nuclear staining of TDP-43 is lost in neuronal cells with inclusions in diseased brains (Nonaka et al. 2009b). Furthermore, we identified two cleavage sites of TDP-43 deposited in FTLD-U by mass spectrometric analysis, and confirmed that expression of these fragments as GFP fusions also afforded cytoplasmic inclusions positive for ubiquitin and phosphorylated TDP-43 (Nonaka et al. 2009b). The cleavage sites identified in the 23-kDa C-terminal fragment of FTLD were different from that of caspase-3, suggesting that caspase is not the enzyme responsible for generating the 23-kDa fragment (Nonaka et al. 2009b). These cellular models recapitulate many of the features of TDP-43 in patients, and therefore, should be useful for screening small molecules for activity to inhibit TDP-43 aggregate formation. We tested whether or not methylene blue and dimebon have the ability to suppress formation of pathological TDP-43 inclusions. Compared to controls, a 50% reduction in the number of inclusions with 0.05 μM methylene blue, a 45% reduction with 5 μM dimebon and an 80% reduction with the combination of 0.05 μM methylene blue and 5 μM dimebon were observed (Yamashita et al. 2009). The effects were statistically significant and the results were also confirmed by Western blotting. These results suggest that these two compounds may be effective in the therapy of ALS, FTLD-U and other TDP-43 proteinopathies.

## TDP-43 C-Terminal Fragments

Based on neuropathological studies, TDP-43 proteinopathies have been classified into 4 subtypes (Cairns et al.

2007). Type 1 is characterized by dystrophic neurites (DNs) with few neuronal cytoplasmic inclusions (NCIs) and no neuronal intranuclear inclusions (NIIs), Type 2 has numerous NCIs with few DNs and no NIIs, Type 3 has numerous NCIs and DNs and occasional NIIs and Type 4 has numerous NIIs and DNs with few NCIs, a pattern which is specific for familial FTLD-U with mutations of VCP gene. There appears to be a strong relationship between other subtypes of TDP-43 pathology and clinical phenotype. Type 1 is associated with semantic dementia, type 2 with FTLD with motor neuron disease (MND), ALS or clinical signs of MND, and type 3 with progressive nonfluent aphasia or FTD with mutation in the progranulin gene. Recent studies of ALS have clarified the wide distribution of neuronal and glial TDP-43 pathology in multiple areas of the central nervous systems (Geser et al. 2008; Nishihira et al. 2009), suggesting that ALS does not selectively affect only the motor system, but rather is a multisystem neurodegenerative TDP-43 proteinopathy affecting both neurons and glial cells.

By immunoblot analyses of the Sarkosyl-insoluble fractions from FTLD-U and ALS patients, we found that the band patterns of the C-terminal fragments of phosphorylated TDP-43 corresponded to the neuropathological subtypes. Type 1 FTLD-U showed two major bands at 23 and 24 kDa and two minor bands at 18 and 19 kDa, while type 2 ALS showed three major bands at 23, 24 and 26 kDa and two minor bands at 18 and 19 kDa. Type 3 FTD with mutation in the progranulin gene showed an intermediate pattern between those two. These results clearly indicate that TDP-43 proteinopathies subclassified by neuropathological differences can also be distinguished biochemically. This strong association between the neuropathology and the biochemistry is critical for understanding the molecular pathogenesis of TDP-43 proteinopathies.

## Biochemical Analysis of TDP-43 in FTLD-U and ALS

The biochemical differences of TDP-43, as shown in the different band patterns of TDP-43 C-terminal fragments, are closely linked to the morphologies of inclusions. The properties of the abnormal TDP-43 may determine the neuropathological and clinical phenotypes of TDP-43 proteinopathies. Similar biochemical and neuropathological differences have been reported in tau between PSP and CBD. Both PSP and CBD are tauopathies with deposition of 4-repeat tau isoforms; however, distinct types of C-terminal fragments are detected, i.e., a 33-kDa band in PSP and ~3-kDa bands in CBD (Arai et al. 2004).

So, what do the different band patterns mean? It is clear that the fragments are produced by cleavage at multiple sites of TDP-43. The band patterns also suggest that the cleavage sites are slightly altered between the diseases. Based on these observations, it is likely that the event may occur after the assembly or aggregation of abnormal TDP-43, and represent relatively protease-resistant domains of TDP-43, which form beta-sheet structure. That is, the different band patterns in TDP-43 proteinopathies represent different conformations of abnormal TDP-43 in the diseases.

To test this idea, we performed protease treatment of the abnormal TDP-43 recovered in the Sarkosyl-insoluble pellets, and analyzed the protease-resistant bands. Proteins can be easily cleaved by proteases if they are denatured or unstructured, but domains that have rigid structures such as beta-sheet structure, or that are structurally buried or interacting with other molecules, are highly resistant to proteases. Figure 1 shows the result of immunoblot analysis of abnormal TDP-43 from two ALS and two FTLD-U cases before and after protease treatment. Before treatment, hyperphosphorylated full-length TDP-43 at 45 kDa, smearing substances and 18–26 kDa C-terminal fragments were detected by pS409/410. The band patterns of the C-terminal fragments are different between FTLD-U with type 1 pathology and ALS with type 2 pathology. Upon trypsin or chymotrypsin treatment, the full-length 45-kDa band and smearing substance of TDP-43 disappeared and protease-resistant core fragments appeared at 16–26 kDa (Fig. 1). As expected, the protease-resistant band pattern of ALS is different and clearly distinguishable from that of FTLD-U. Doublet bands at ~16 kDa and a band at 25 kDa were detected in ALS, but only a single broad band at ~16 kDa was detected in FTLD-U with type 1 pathology after trypsin treatment (Fig. 1). Similarly, multiple protease-resistant bands were detected at 16–25 kDa after chymotrypsin treatment and the band patterns were different between ALS and FTLD-U (Fig. 1). These results strongly support the idea that the different band patterns of the C-terminal fragments reflect different conformations of abnormal TDP-43 molecules between ALS and FTLD-U.

## TDP-43 in Different Brain Regions

Similar protease-resistant bands and differences in the band patterns have been reported in prion diseases, CJD and BSE (Collinge et al. 1996). Protease-resistant prion from new-variant CJD cases showed a different characteristic pattern from that in sporadic CJD cases, and the band pattern is indistinguishable from that of mice infected with BSE prion. This is biochemical evidence that the BSE agent has been transmitted from bovine to human.

Applying this to TDP-43 in TDP-43 proteinopathies, it is possible to determine whether there is any difference between the abnormal TDP-43 accumulated in cortex and that in spinal cord by analyzing the band patterns of the C-

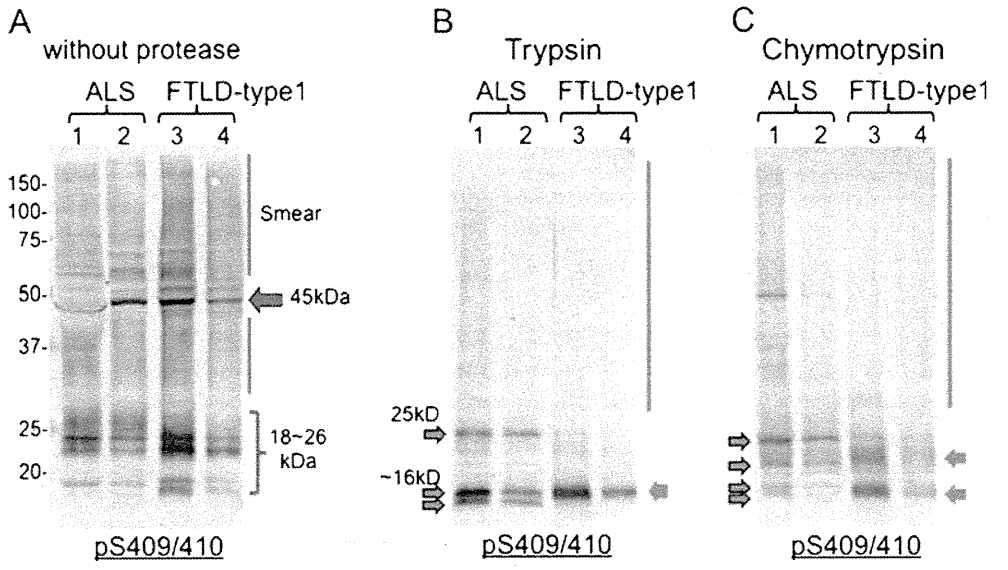


**Fig. 1** Immunoblot analysis of abnormal TDP-43 from two ALS and two FTLD-U cases before and after protease treatment with a phosphorylation dependent anti-TDP-43 rabbit polyclonal antibody (pS409/410). **a** Hyperphosphorylated full-length TDP-43 at 45 kDa, smearing substances and 18–26 kDa C-terminal fragments were detected by pS409/410 before treatment. The band patterns of the C-terminal fragments are different between FTLD-U with type 1 pathology and ALS with type 2 pathology. **b** Upon trypsin treatment, the full-length 45 kDa band and smearing substance of TDP-43 disappeared and protease-resistant core fragments appeared at 16~26 kDa. Doublet bands at ~16 kDa and a band at 25 kDa were seen in ALS, but a single broad band at ~16 kDa was detected in FTLD-U with type 1 pathology after trypsin treatment. **c** Multiple protease-resistant bands were detected at 16~25 kDa after chymotrypsin treatment and the band patterns were different between ALS and FTLD-U

terminal fragments of TDP-43. Thus, we have prepared Sarkosyl-insoluble fractions from cortex and spinal cords of three ALS cases, immunoblotted them with pS409/410 and compared the results. In all three cases, type 2 C-terminal fragments of TDP-43 were detected, and there was no significant difference between the band pattern in cortex and that in spinal cord (data not shown). This strongly suggests that the same form of abnormal TDP-43 molecule is deposited in different brain regions. Similar results were also obtained from the analysis of the C-terminal band pattern of TDP-43 in FTLD-U. It seems highly unlikely that the same conformational change would occur synchronously in different brain regions. Instead, it seems more likely that abnormal protein produced in cells is transferred to different regions and propagated. These biochemical data obtained from the brains of patients provide biochemical evidence that abnormal species of TDP-43 are transmitted from cell to cell and propagated in vivo.

## Discussion

Amyloid-like protein deposition is a common neuropathological feature of many neurodegenerative diseases. Hyperphosphorylated tau in Alzheimer's disease and related tauopathies, hyperphosphorylated alpha-synuclein in Parkinson's disease and other alpha-synucleinopathies, and expanded polyglutamines in polyglutamine diseases have been identified. Importantly, the extent of the abnormal protein pathologies is closely correlated with the disease progression (Braak and Braak 1991; Braak et al. 2003; Saito et al. 2003). The proteins or protein fibrils deposited in cells in these diseases have been shown to have a common structural feature. Cross-beta structure, which is the same as in abnormal prion protein, has been demonstrated in filaments or fibrils composed of tau (Berriman et al. 2003), alpha-synuclein (Serpell et al. 2000) or expanded polyglutamines (Perutz 1999). It has not been demonstrated in TDP-43 yet, but we have shown by electron microscopy that phosphorylated TDP-43 in motor neurons of ALS patients has a fibrous structure (Hasegawa et al. 2008), suggesting that TDP-43 is also an amyloid-like protein.

For the assembly of amyloid fibrils, nucleation-dependent protein polymerization has been proposed. This comprises nucleation and elongation phases, and nucleation is the rate-limiting step. It takes a long time to form the first aggregated seed from the monomer, but once the seed is formed, the elongation step proceeds relatively quickly. More importantly, by addition of amyloid-seed, proteins are often converted to the same conformation as that of the seed. For example, WT monomeric alpha-synuclein is converted to A30P-type amyloid fibrils when it is incubated with a small amount of fibril-seeds formed with A30P mutant alpha-synuclein (Yonetani et al. 2009). Differences in the conformations of the amyloid fibrils are detected based on the differences in the protease-resistant band

patterns, as in the typing of prion proteins. There is another example of nucleation-dependent amyloid fibril formation in cultured cells. We developed a novel method for introducing amyloid seeds into cultured cells using lipofectoamine, and presented experimental evidence of seed-dependent polymerization of alpha-synuclein, leading to the formation of filamentous protein deposits and cell death (Nonaka et al. 2010). Overexpression of alpha-synuclein itself in cells does not generate abnormal inclusions, but if fibril seeds formed with alpha-synuclein are introduced into cells, abundant filamentous alpha-synuclein aggregates positive for PSer129 and ubiquitin are developed, and cells with inclusions undergo cell death. This was also clearly demonstrated in cells expressing different tau isoforms by introducing the corresponding tau fibril seeds (Nonaka et al. 2010).

The above results obtained from biochemical analyses of abnormal proteins in patients strongly suggest that intracellular amyloid-like proteins, including TDP-43, propagate from cell to cell and this propagation is the cause of disease progression, analogously to metastasis of cancer cells to multiple different tissues in cancer progression. From this point of view, we have proposed as a hypothesis that neurodegenerative diseases with amyloid-like proteins can be regarded as "protein cancers." The term prion, coined in 1982 by Stanley B. Prusiner, describes an agent transmissible among humans and a variety of mammals. On the other hand, the term "protein cancers" describes diseases that involve the spreading or propagation of abnormal proteins in tissues or individuals, even though the mechanism of propagation is basically the same as that of prions. Amyloid-like protein interacts with normal protein and converts it to the same abnormal conformation, and the amplified amyloid-like protein is transmitted from cell to cell, probably through synapses, and propagates to various brain regions (Fig. 2). As a result, the same abnormal protein pathology expands gradually, and clinical manifestations that are associated with affected brain regions become more marked because of the transmission and propagation of the abnormal protein. Therefore, it is important to regulate the propagation of abnormal proteins for clinical therapy.

## Conclusions

1. In ALS, FTLD-U and other TDP-43 proteinopathies, abnormally phosphorylated, ubiquitinated, and truncated TDP-43 is accumulated in a filamentous form.
2. We established cellular models which recapitulate many of the features of the abnormal TDP-43 in FTLD-U and ALS
3. ALS-related pathogenic mutations of the TDP-43 gene accelerate aggregate formation by the C-terminal fragments.
4. The band pattern of the TDP-43 C-terminal fragments is different between diseases with different clinicopathological phenotypes, and it represents different conformations of the abnormal TDP-43 between the diseases.
5. The C-terminal band patterns in several brain areas and spinal cord in each individual case of sporadic ALS are indistinguishable.
6. These and other results suggest that abnormal TDP-43, tau and alpha-synuclein are transmitted and propagated from cell to cell in different regions during disease progression. It is important to find drugs that can block the propagation of abnormal proteins for clinical therapy.

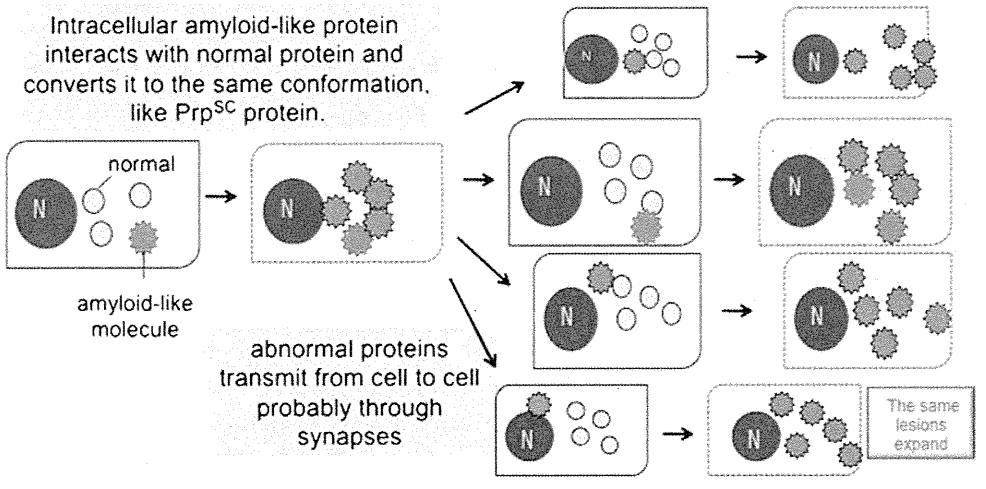


**Fig. 2** Schematic representation of prion-like conversion of normal protein into amyloid-like protein and its propagation in neurodegenerative diseases. Intracellular amyloid-like protein interacts with normal protein and converts it to the same abnormal conformation. Amplified abnormal amyloid-like protein is transmitted from cell to cell, probably through synapses, and propagates to various brain regions. As a result, the same abnormal protein pathology expands gradually, and clinical manifestations that are associated with affected brain regions become more marked because of the transmission and propagation of the abnormal protein. From this point of view, neurodegenerative diseases with amyloid-like proteins can be regarded as 'protein cancers"

## References


Amador-Ortiz C, Lin WL, Ahmed Z et al (2007) TDP-43 immunoreactivity inhippocampal sclerosis and Alzheimer's disease. Ann Neurol 61:435–445

Arai T, Ikeda K, Akiyama H, Nonaka T, Hasegawa M, Ishiguro K et al (2004) Identification of amino-terminally cleaved tau fragments that distinguish progressive supranuclear palsy from corticobasal degeneration. Ann Neurol 55:72–79

Arai T, Hasegawa M, Akiyama H et al (2006) TDP-43 is a component of ubiquitin-positive tau-negative inclusions in frontotemporal lobar degeneration and amyotrophic lateral sclerosis. Biochem Biophys Res Commun 351:602–611

Arai T, Mackenzie IR, Hasegawa M et al (2009) Phosphorylated TDP-43 in Alzheimer's disease and dementia with Lewy bodies. Acta Neuropathol 117:125–136

Ayala YM, Pantano S, D'Ambrogio A et al (2005) Human, *Drosophila*, and *C. elegans* TDP43: nucleic acid binding properties and splicing regulatory function. J Mol Biol 348:575–588

Barmada SJ, Finkbeiner S (2010) Pathogenic TARDBP mutations in amyotrophic lateral sclerosis and frontotemporal dementia: disease-associated pathways. Rev Neurosci 21:251–272 (Review)

Benajiba L, Le Ber I, Camuzat A, Lacoste M et al (2009) TARDBP mutations in motoneuron disease with frontotemporal lobar degeneration. Ann Neurol 65:470–473

Berriman J, Serpell LC, Oberg KA et al (2003) Tau filaments from human brain and from in vitro assembly of recombinant protein show cross-beta structure. Proc Natl Acad Sci USA 100:9034–9038

Borroni B, Bonvicini C, Alberici A et al (2009) Mutation within TARDBP leads to frontotemporal dementia without motor neuron disease. Hum Mutat 30:E974–E983

Bose JK, Wang IF, Hung L, Tarn WY, Shen CK (2008) TDP-43 overexpression enhances exon 7 inclusion during the survival of motor neuron pre-mRNA splicing. J Biol Chem 283:28852–28859

Braak H, Braak E (1991) Neuropathological staging of Alzheimer-related changes. Acta Neuropathol 82:239–259

Braak H, Del Tredici K, Rub U, de Vos RA et al (2003) Staging of brain pathology related to sporadic Parkinson's disease. Neurobiol Aging 24:197–211

Buratti E, Brindisi A, Giombi M, Tisminetzky S, Ayala YM, Baralle FE (2005) TDP-43 binds heterogeneous nuclear ribonucleoprotein A/B through its C-terminal tail. J Biol Chem 280:37572–37584

Cairns NJ, Bigio EH, Mackenzie IR et al (2007) Neuropathologic diagnostic and nosologic criteria for frontotemporal lobar degeneration: consensus of the Consortium for Frontotemporal Lobar Degeneration. Acta Neuropathol 114:5–22

Collinge J, Sidle KC, Meads J, Ironside J, Hill AF (1996) Molecular analysis of prion strain variation and the aetiology of 'new variant' CJD. Nature 383:685–690

Freeman SH, Spires-Jones T, Hyman BT, Growdon JH, Frosch MP (2008) TAR-DNA binding protein 43 in Pick disease. J Neuropathol Exp Neurol 67:62–67

Fujishiro H, Uchikado H, Arai T et al (2009) Accumulation of phosphorylated TDP-43 in brains of patients with argyrophilic grain disease. Acta Neuropathol 117:151–158

Geser F, Winton MJ, Kwong LK et al (2007) Pathological TDP-43 in parkinsonism-dementia complex and amyotrophic lateral sclerosis of Guam. Acta Neuropathol 115:133–145

Geser F, Brandmeir NJ, Kwong LK et al (2008) Evidence of multisystem disorder in whole-brain map of pathological TDP-43 in amyotrophic lateral sclerosis. Arch Neurol 65:636–641

Gitcho MA, Baloh RH, Chakraverty S et al (2008) TDP-43 A315T mutation in familial motor neuron disease. Ann Neurol 63:535–538

Hasegawa M, Arai T, Akiyama H et al (2007) TDP-43 is deposited in the Guam parkinsonism-dementia complex brains. Brain 130:1386–1394

Hasegawa M, Arai T, Nonaka T et al (2008) Phosphorylated TDP-43 in frontotemporal lobar degeneration and amyotrophic lateral sclerosis. Ann Neurol 64:60–70

Higashi S, Iseki E, Yamamoto R et al (2007) Concurrence of TDP-43, tau and alpha-synuclein pathology in brains of Alzheimer's disease and dementia with Lewy bodies. Brain Res 1184:284–294

Kabashi E, Valdmanis PN, Dion P et al (2008) TARDBP mutations in individuals with sporadic and familial amyotrophic lateral sclerosis. Nat Genet 40:572–574

Lin WL, Dickson DW (2008) Ultrastructural localization of TDP-43 in filamentous neuronal inclusions in various neurodegenerative diseases. Acta Neuropathol 116:205–213

Nakashima-Yasuda H, Uryu K, Robinson J et al (2007) Co-morbidity of TDP-43 proteinopathy in Lewy body related diseases. Acta Neuropathol 114:221–229

Neumann M, Sampathu DM, Kwong LK et al (2006) Ubiquitinated TDP-43 in frontotemporal lobar degeneration and amyotrophic lateral sclerosis. Science 314:130–133

Nishihira Y, Tan CF, Hoshi Y et al (2009) Sporadic amyotrophic lateral sclerosis of long duration is associated with relatively mild TDP-43 pathology. Acta Neuropathol 117:45–53

Nonaka T, Arai T, Buratti E, Baralle FE, Akiyama H, Hasegawa M (2009a) Phosphorylated and ubiquitinated TDP-43 pathological inclusions in ALS and FTLD-U are recapitulated in SH-SY5Y cells. FEBS Lett 583:394–400

Nonaka T, Kametani F, Arai T, Akiyama H, Hasegawa M (2009b) Truncation and pathogenic mutations facilitate the formation of intracellular aggregates of TDP-43. Hum Mol Genet 18:3353–3364

Nonaka T, Watanabe ST, Iwatsubo T, Hasegawa M (2010) Seeded aggregation and toxicity of alpha-synuclein and tau: cellular models of neurodegenerative diseases. J Biol Chem 285:34885–34898

Perutz MF (1999) Glutamine repeats and neurodegenerative diseases. Brain Res Bull 50:467

Pesiridis GS, Lee VM, Trojanowski JQ (2009) Mutations in TDP-43 link glycine-rich domain functions to amyotrophic lateral sclerosis. Hum Mol Genet 18:R156–R162

Saito Y, Kawashima A, Ruberu NN, Fujiwara H et al (2003) Accumulation of phosphorylated alpha-synuclein in aging human brain. J Neuropathol Exp Neurol 62:644–654

Serpell LC, Berriman J, Jakes R et al (2000) Fiber diffraction of synthetic alpha-synuclein filaments shows amyloid-like cross-beta conformation. Proc Natl Acad Sci USA 97:4897–4902

Sreedharan J, Blair IP, Tripathi VB et al (2008) TDP-43 mutations in familial and sporadic amyotrophic lateral sclerosis. Science 319:1668–1672

Uryu K, Nakashima-Yasuda H, Forman MS et al (2008) Concomitant TAR-DNA-binding protein 43 pathology is present in Alzheimer disease and corticobasal degeneration but not in other tauopathies. J Neuropathol Exp Neurol 67:555–564

Van Deerlin VM, Leverenz JB, Bekris LM et al (2008) TARDBP mutations in amyotrophic lateral sclerosis with TDP-43 neuropathology: a genetic and histopathological analysis. Lancet Neurol 7:409–416

Yamashita, M., Nonaka, T., Arai, T et al (2009) Methylene blue and dimebon inhibit aggregation of TDP-43 in cellular models. FEBS Lett 583:2419–24

Yokoseki A, Shiga A, Tan CF et al (2008) TDP-43 Mutation in familial amyotrophic lateral sclerosis. Ann Neurol 63:538–542

Yonetani M, Nonaka T, Masuda M et al (2009) Conversion of wild-type alpha-synuclein into mutant-type fibrils and its propagation in the presence of A30P mutant. J Biol Chem 284:7940–7950

*Neuroscience* 177 (2011) 298–307

# EFFECT OF GLYCOGEN SYNTHASE KINASE 3 β-MEDIATED PRESENILIN 1 PHOSPHORYLATION ON AMYLOID β PRODUCTION IS NEGATIVELY REGULATED BY INSULIN RECEPTOR CLEAVAGE

**M. MAESAKO,[a] K. UEMURA,[b] M. KUBOTA,[a] K. HIYOSHI,[a] K. ANDO,[b] A. KUZUYA,[b] T. KIHARA,[c] M. ASADA,[a] H. AKIYAMA[d] AND A. KINOSHITA[a]***

[a]*School of Human Health Sciences, Kyoto University Graduate School of Medicine, Kyoto 606-8507, Japan*

[b]*Department of Neurology, Kyoto University Graduate School of Medicine, Kyoto 606-8507, Japan*

[c]*Department of Neuroscience for Drug Discovery, Kyoto University Graduate School of Pharmaceutical Sciences, Kyoto 606-8501, Japan*

[d]*Tokyo Institute of Psychiatry, Tokyo 156-8585, Japan*

**Abstract—Presenilin 1 (PS1), a causative molecule of familial Alzheimer's disease (AD), is known to be an unprimed substrate of glycogen synthase kinase 3 β (GSK3β) [Twomey and McCarthy (2006) FEBS Lett 580:4015–4020] and is phosphorylated at serine 353, 357 residues in its cytoplasmic loop region [Kirschenbaum et al. (2001) J Biol Chem 276:7366–7375]. In this report, we investigated the effect of PS1 phosphorylation on AD pathophysiology and obtained two important results—PS1 phosphorylation increased amyloid β (Aβ) 42/40 ratio, and PS1 phosphorylation was enhanced in the human AD brains. Interestingly, we demonstrated that PS1 phosphorylation promoted insulin receptor (IR) cleavage and the IR intracellular domain (IR ICD) generated by γ-secretase led to a marked transactivation of Akt (PKB), which down-regulated GSK3β activity. Thus, the cleavage of IR by γ-secretase can inhibit PS1 phosphorylation in the long run. Taken together, our findings indicate that PS1 phosphorylation at serine 353, 357 residues can play a pivotal role in the pathology of AD and that the dysregulation of this mechanism may be causally associated with its pathology.** © 2011 IBRO. Published by Elsevier Ltd. All rights reserved.

**Key words: Alzheimer's disease, presenilin 1, phosphorylation, regulated intramembrane proteolysis, insulin receptor, Akt.**

Alzheimer's disease (AD) is pathologically characterized by amyloid plaques and neurofibrillary tangles (NFTs). Amyloid plaques are composed of amyloid β (Aβ) peptides, which are derived from amyloid precursor protein (APP) via proteolytic cleavage by γ-secretase (De Strooper et al., 1998). γ-Secretase is an enzymatic complex composed of at least four proteins: Presenilin 1 or Presenilin 2 (PS1 or PS2), Nicastrin, Pen 2, and Aph 1, with Presenilin representing the catalytic core (Yu et al., 2000; Francis et al., 2002; Goutte et al., 2002). PS1 mutations account for the majority of cases of familial AD, and more than 170 pathogenic mutations have been identified within the PS1 coding sequence. On the other hand, NFTs are characterized by the accumulation of hyperphosphorylated Tau in neurons (Grundke-Iqbal et al., 1986). One of the candidates which phosphorylate Tau is glycogen synthase kinase 3 β (GSK3β) (Hanger et al., 1992).

GSK3β, originally known to inactivate glycogen synthesis, is a serine/threonine protein kinase with a wide variety of substrates, and is expressed in various tissues with the highest level in the brain (Grundke-Iqbal et al., 1986). Interestingly, GSK3β phosphorylates not only Tau but also PS1 at serine 353, 357 residues in its cytoplasmic loop region (Kirschenbaum et al., 2001; Twomey and McCarthy, 2006). Therefore, it is intriguing to examine the function of PS1 phosphorylation at those residues to connect two AD hallmarks—amyloid plaques and NFTs. Although our recent report demonstrated that GSK3β-mediated PS1 phosphorylation regulates the localization of γ-secretase and inhibits its N-cadherin cleavage (Uemura et al., 2007), a direct impact of PS1 phosphorylation on AD pathogenesis has not been elucidated so far.

Here, we demonstrate that GSK3β-mediated PS1 phosphorylation inhibits APP cleavage by γ-secretase activity and decreases the total Aβ production whereas it increases Aβ 42/40 ratio. Importantly, we found that PS1 phosphorylation was enhanced in the human AD brains. To further elucidate the underlying mechanisms which regulate PS1 phosphorylation, we focused on insulin signaling. We observed that phosphorylated PS1 promotes the cleavage of insulin receptor (IR) by γ-secretase activity. Intracellular domain of IR (IR ICD), produced by the cleavage, enhances the transcription of Akt (PKB), leading to inhibit GSK3β activity. Therefore, we propose that PS1, localized downstream of GSK3β, may play a pivotal role in Aβ production under the influence of insulin signaling, a mechanism that may be deeply associated with AD pathophysiology.

## EXPERIMENTAL PROCEDURES

### Human brain samples

From the brain tissue collection in Tokyo Institute of Psychiatry (H.A.), which mainly consists of cases from psychogeriatric wards, we employed experiments of six dementia patients' brains with CERAD plaque score "C" (Mirra et al., 1991) and Braak and

*Corresponding author. Tel: +81-75-751-3969; fax: +81-75-751-3969.
E-mail address: akinoshita@hs.med.kyoto-u.ac.jp (A. Kinoshita).

*Abbreviations:* AD, Alzheimer's disease; APP, amyloid precursor protein; Aβ, amyloid β; CTF, C-terminal fragment; FBS, fetal bovine serum; GSK3β, glycogen synthase kinase 3 β; ICD, intracellular domain; IR, insulin receptor; MEF, mouse embryonic fibroblast; NFTs, neurofibrillary tangles; NTF, N-terminal fragment; PS1, presenilin 1; RIP, regulated intramembrane proteolysis.

0306-4522/11 $ - see front matter 
doi:10.1016/j.neuroscience.2010.12.017

**Table 1.** Characteristics of human brain samples

| | Case | Age (y) | Sex | Postmortem interval (h) | Clinical diagnosis | Pathological findings |
|---|---|---|---|---|---|---|
| 1 | Schizophrenia | 75 | M | 15 | Schizophrenia | Plaque(−), NFT stage II, minor stroke |
| 2 | Aortic rupture | 80 | F | 2 | Aortic rupture | Plaque(−), tangle(−) |
| 3 | Cirrhosis of the liver | 77 | M | 7.5 | Cirrhosis of the liver | Plaque(−), NFT stage I |
| 4 | Alcoholism | 60 | M | 5 | Alcoholism | Plaque(−), tangle(−) |
| 5 | Fahr disease | 48 | M | 10 | Fahr disease | Plaque(−), tangle(−) |
| 6 | AD① | 75 | M | 12 | Alzheimer's disease | Braak stage C, VI |
| 7 | AD② | 68 | F | 9 | Alzheimer's disease | Braak stage C, VI |
| 8 | AD③ | 75 | M | 17.5 | Alzheimer's disease | Braak stage C, VI |
| 9 | AD④ | 77 | M | 2 | Alzheimer's disease | Braak stage C, VI |
| 10 | AD⑤ | 87 | F | 6 | Alzheimer's disease | Braak stage C, VI |
| 11 | AD⑥ | 56 | M | 18 | Alzheimer's disease | Braak stage C, VI |

We employed experiments of six Alzheimer's disease patients' brains, as well as five control subjects without neurological complications. Fresh-frozen samples were taken in all cases from the mediobasal temporal neocortex. There is no statistical difference in the postmortem interval between AD and control cases.

Braak's NFTs stage IV or higher (Braak and Braak, 1991), as those with AD, as well as five control subjects without neurological complications (Table 1). Fresh-frozen samples were taken in all cases from the mediobasal temporal neocortex. The brain samples were extracted in RIPA buffer (50 mM Tris–HCl, 150 mM NaCl, 1% Triton X100, 1% NP-40, 0.5% Deoxycholate, 0.1% SDS, pH 8.0) with protease inhibitor cocktail (Roche, Switzerland) and sufficiently homogenized on ice. Then the samples were incubated for one night at 4 °C and centrifuged at 14,000 g×20 min. The supernatants were directly used for Western blot analysis. All autopsies were undertaken with written consents and the study was approved by the official ethical committees of Kyoto University as well as of Tokyo Institute of Psychiatry.

## Plasmid constructs

The pcDNA3.1-hIR (human Insulin Receptor) construct was a kind gift from Dr. Ikeuchi (Niigata University, Japan) (Ebina et al., 1985). The cDNA encoding the IR ICD was generated by polymerase chain reaction (PCR) using the following primers: IR ICD forward, CGGGTACCCGCCATGAGAAAGAGGCAGCCAGA, and IR ICD reverse, CGGGATCCGGAAGGATTGGACCGAGGCAA. The PCR product was subcloned into the reading frame of the Kpn1/BamH1 sites of the pcDNA3 with HA tag vector. The construction of the plasmids expressing wt PS1, pseudo-phosphorylation PS1 (S353/357D PS1), deletion mutant PS1 (Δ340-350 PS1), and dominant negative PS1 (D385A PS1) was described previously (Uemura et al., 2003, 2007). Precise cloning of all reading frames was verified by sequencing.

## Cell culture and transfection

SH-SY5Y (derived from human neuroblastoma) cells were maintained in Opti-MEM containing 10% fetal bovine serum (FBS) (Invitrogen, USA). Establishment of cell lines which stably express hIR was described previously (Maesako et al., 2010). PS1/PS2 double knockout mouse embryonic fibroblast (MEF PS-/-) cells were generously donated by Dr. B De Strooper and they were maintained in Dulbecco's modified Eagle's medium (DMEM) (SIGMA, USA) with 10% FBS. CHO cells stably expressing both Swedish mutant APP (K670M/N770L) and human N-cadherin (APPsw/Ncad-CHO cells) were obtained and maintained as described previously (Uemura et al., 2007). For transient transfection into SH-SY5Y as well as into MEF PS-/- cells, cells were plated in 6-cm dishes with serum-containing medium. 8 μg of plasmid DNA and 20 μl of TransFectin reagent (Bio-Rad, USA) were mixed into 1 ml of serum-free medium and incubated for 20 min, then added directly to confluent cells in 2 ml of serum-containing medium. 24 to 48 h after transfection, reporter gene activity was assayed.

## Antibodies and chemical reagents

Anti-IR, a monoclonal antibody recognizing the C-terminal amino acid residues of human IR, was from Neo Markers. Rabbit polyclonal anti-Akt and phospho-GSK3β (S9) were from Cell Signaling Technology. Mouse monoclonal anti-GSK3β was from BD Transduction Laboratories. Mouse monoclonal anti-β-actin and rabbit polyclonal anti-APP C-terminal antibodies were from SIGMA. Rabbit polyclonal anti-PS1 NTF and goat polyclonal phospho-PS1 (S353/357) antibodies were from Santa Cruz. Mouse monoclonal PS1 CTF antibody was from Calbiochem. Alexa Fluor 546 anti-mouse IgG and Alexa Fluor 488 anti-goat IgG were obtained from Molecular Probes. γ-secretase inhibitor DAPT and L-685458 were from SIGMA. Akt inhibitor IV, TPA, and PKC inhibitor were from Calbiochem. Insulin solution was from SIGMA and DMSO was from Nacalai tesque.

## Western blotting

Cells were washed in phosphate-buffered saline (PBS) two times and scraped off. Cell pellets were suspended in ice-cold TNE buffer (10 mM Tris–HCl, 150 mM NaCl, 1% NP-40, 1 mM EDTA pH 7.8), supplemented with protease inhibitor cocktail, and briefly subjected to sonication. The samples were centrifuged at 14,000 g×20 min at 4 °C and the supernatants were collected to obtain protein samples. The protein concentration was determined using the Bradford assay (Bradford, 1976). Protein samples were diluted with sample buffer (125 mM Tris, 4% SDS, 2% 2-mercaptoethanol, 20% glycerol and 0.01% Bromophenol Blue, pH 6.8) and denatured at 95 °C for 5 min. Samples containing equal amounts of protein were electrophoresed on polyacrylamide gradient gels (5–20%) (Atto, Japan) in running buffer (25 mM Tris, 192 mM glycine, 0.1% SDS). In this gel, APP C-terminal fragments (CTFs) bands were shown as a single band. To detect APP ICD (AICD), samples were electrophoresed on 15% Tricine gels (Atto, Japan) in Tricine SDS Running Buffer. Immunoblotting was carried out by transferring the proteins to polyvinylidene difluoride microporous membrane, blocking this membrane with 5% skimmed milk in 20 mM TBS containing 0.1% Tween 20 (TBS-T), and incubating with the primary antibodies in PBS containing 4% bovine serum albumin (BSA) (Nacalai tesque, Japan) overnight at 4 °C. The membranes were then washed in TBS-T and incubated with a horseradish peroxidase-conjugated anti-mouse IgG (GE Healthcare, UK) in TBS-T for 1 h at room temperature. The specific reaction

was visualized using the enhanced chemiluminescence (ECL) method (GE Healthcare).

### *In vitro* γ-secretase assay

To analyze AICD or IR ICD level by *in vitro* γ-secretase assay (Sastre et al., 2001), cells were suspended (0.5 ml/10 cm dish) in homogenization buffer (10 mM MOPS, 10 mM KCl, pH 7.0) and homogenates and the post-nuclear supernatant (PNS) were prepared as described (Steiner et al., 1998). Membranes were pelleted from the PNS by centrifugation for 20 min at 16,000 g at 4 °C, washed with homogenization buffer and resuspended (50 μl/10 cm dish) in assay buffer (150 mM sodium citrate, pH 6.4). To allow generation of ICD, samples were incubated at 37 °C for 2 h in a volume of 25 μl/ assay. Control samples were kept at 4 °C. After termination of the assay reactions, samples were separated into pellet fractions (membrane fractions) and supernatant fractions by ultracentrifugation for 1 h at 100,000 g at 4 °C. AICD was detected using polyclonal anti-APP C-terminal antibody and IR ICD was detected using monoclonal anti-IR C-terminal antibody.

### Immunostaining

$5.0\times10^4$ cells were harvested onto 0.1% polyethyleneimine-coated Lab-Tek II Chamber slides (four-well; Nalge Nunc International, Rochester) and maintained in Opti-MEM containing 10% FBS. Cells were cultured for the indicated time and then fixed with 4% paraformaldehyde for 20 min. Fixed cells were blocked with PBS containing 0.2% Triton X-100 for 15 min and incubated overnight at 4 °C with each antibody diluted in PBS containing 3% BSA. Immunoreactivity was visualized using the species-specific secondary antibodies mentioned above. The samples were examined using a laser confocal scanning microscope, LSM 510 Pascal (Zeiss, Switzerland).

### Measurement of extracellular Aβ

The levels of Aβ 40 and Aβ 42 were measured by ELISA kits specific to Aβ 40 and Aβ 42 (Wako, Japan), as described previously (Uemura et al., 2009). Briefly, APPsw/Ncad-CHO cells were cultured in 6 cm dishes at a density of $7.0\times10^5$ cells /well. 24 h after incubation, the cells were treated with reagents for 5 h in DMEM/F-12 medium, followed by replacing DMEM/F-12 with 6 ml of Opti-MEM. 1 h after replacing, 1 ml of medium was collected, centrifuged at 600 g for 5 min, and 100 μl of the aliquot was used for measurement of extracellular Aβ.

### MTT assay

The viability in APPswe/N-cad-CHO cells was analyzed by MTT assay using MTT Cell Proliferation Assay Kit (Cayman Chemical Co., USA). Briefly, cells were cultured in a 96-well plate at a density of $1.0\times10^4$ cells/well. 24 h after incubation, reagents of indicated concentration were treated for 5 h in the presence of DMEM/F-12 medium, followed by replacing DMEM/F-12 with 100 μl of Opti-MEM with the reagents. 1 h after replacing, MTT was measured using the Kit and microplate reader.

### Real-time PCR assay

Total RNA was isolated using ISOGEN (NIPPON GENE, Japan), according to the manufacture's protocol. For real-time PCR analysis, 5 μg total RNA from each sample was used for cDNA synthesis kit (GE Healthcare). Real-time PCR primers were designed as follows: Akt1: fw GACCTCAAGCTGGAGAAC/rv ACTGCACGGCCGTAGTC, Akt2: fw ACCGCCTGTGCTTTGTGATG/rv TCATTGTCCTCCAGCACCTC, Akt3: fw CATTATTGCAAAGGATGAAGTGGCAC/rv CCAGCATTAGATTCTCCAACTTGAG.

For the amplification of Akt, 5 μl of cDNA was added to the SYBR green master mix (Roche) and real-time PCR assay was performed in LightCycler 480 (Roche).

### Statistical analysis

All values are given in means±SE. Comparisons were performed using an unpaired Student's *t*-test. For comparison of multiparametric analysis, one-way factorial ANOVA, followed by the post hoc analysis by Fisher's PLSD was used. $P<0.05$ was considered to indicate a significant difference. $n=4$ indicated four independent experiments.

## RESULTS

### PS1 phosphorylation inhibits APP cleavage but enhances extracellular Aβ 42/40 ratio

Since PS1 is known to be the essential component of γ-secretase, we examined the effect of its phosphorylation on APP cleavage. To test this, we transfected wt PS1 and pseudo-phosphorylated PS1 mutant S353/357D PS1 (in which serine residues phosphorylated by GSK3β are substituted with aspartate to mimic phosphorylation state; Uemura et al., 2007) into MEF PS-/- cells. Transfected cells were treated with insulin to promote ectodomain shedding (Linda et al., 2007) and to inhibit the phosphorylation of wt PS1 (Maesako et al., 2010). APP CTFs band was accumulated in MEF PS-/- cells (Fig. 1A, first lane). Interestingly, in the absence of insulin, the level of APP CTFs was slightly higher in S353/357D PS1 cells than that in wt PS1 (Fig. 1A, second and third lanes). Moreover, in the presence of insulin, the level of APP CTFs in S353/357D PS1 was significantly increased compared to that in wt PS1 (Fig. 1A, fourth and fifth lanes, Fig. 1B). Using Tricine gels, we could detect that the level of AICD in S353/357D PS1 was decreased compared to that in wt PS1 (Fig. 1C, third and fourth lanes). This result was confirmed by *in vitro* γ-secretase assay (Fig. 1D). Collectively, these results suggested that PS1 phosphorylation inhibited the γ-secretase-mediated cleavage of APP CTFs.

As Aβ plays a pivotal role in the pathogenesis of AD, we next examined the effect of PS1 phosphorylation on extracellular Aβ production, as well as Aβ 42/40 ratio. For this purpose, either Akt inhibitor IV or LiCl, which activates or inhibits GSK3β respectively, was added to change the phosphorylation status of PS1 in APPswe/N-cad-CHO cells (Fig. 1E). Under this condition, neither of them induced cell death (Fig. 1F). Interestingly, Akt inhibitor significantly decreased the amount of extracellular Aβ 40 whereas LiCl significantly increased its amount (Fig. 1G). In contrast, the extracellular Aβ 42 level in the presence of either Akt inhibitor or LiCl remained almost the same (Fig. 1H), thus leading to the increase of Aβ 42/40 ratio in Akt inhibitor-treated cells or to the decrease of its ratio in LiCl-treated cells (Fig. 1I). These results collectively indicate that GSK3β-mediated PS1 phosphorylation down-regulated Aβ production but enhanced Aβ 42/40 ratio.

### PS1 phosphorylation is enhanced in AD human brain samples

It was reported that GSK3β activity was up-regulated in AD brains (Bhat et al., 2004). Therefore, we assumed that the phosphorylation ratio of PS1 might be increased in AD brains. Thus, we analyzed the phosphorylation ratio of PS1

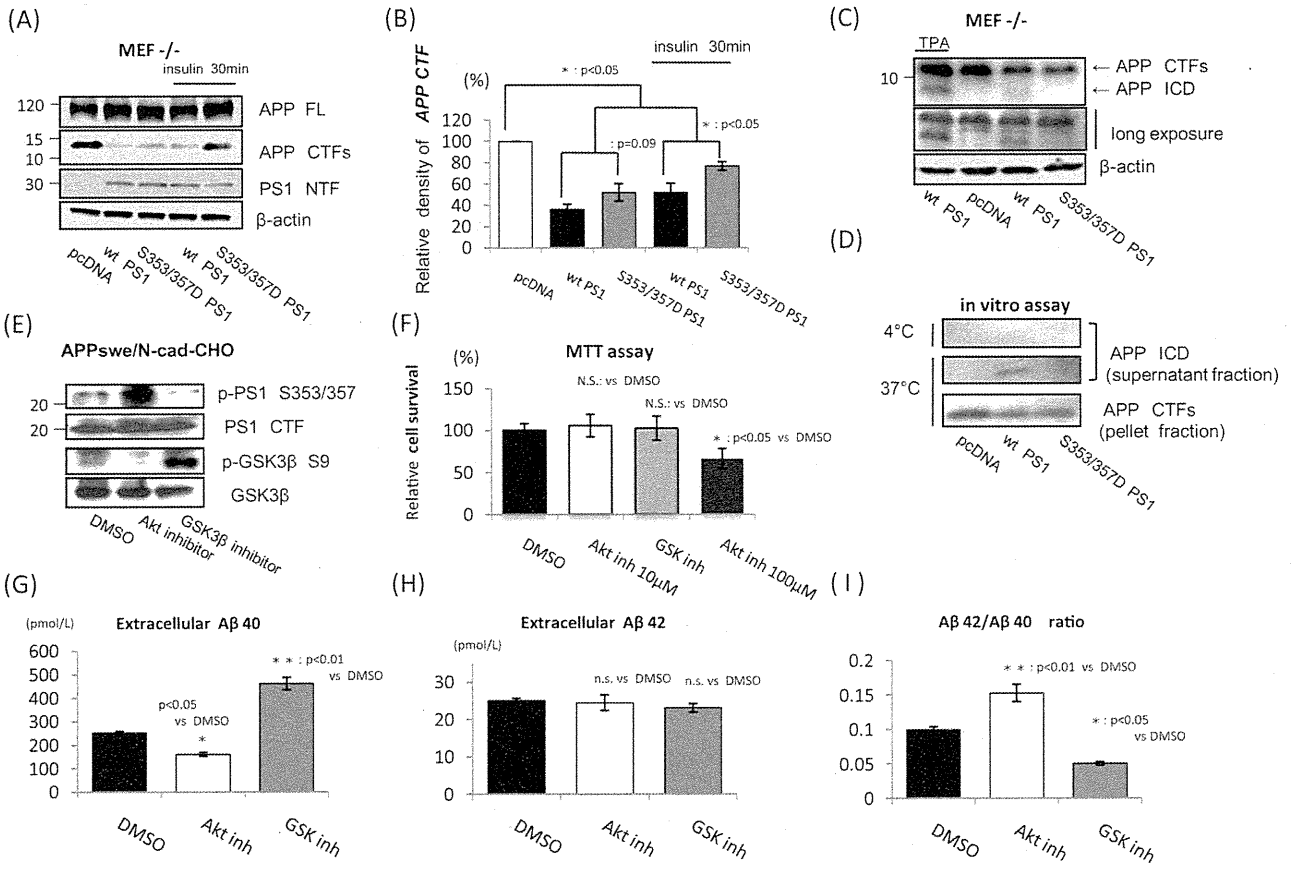


**Fig. 1.** PS1 phosphorylation inhibits APP cleavage but enhances extracellular Aβ 42/40 ratio. (A) Either wt PS1 or pseudo-phosphorylation PS1 mutant (S353/357D PS1) was transfected into MEF PS-/- cells. Control cells were transfected with pcDNA (first lane). 24 h after transfection, cells were treated with 50 nM insulin for 30 min (fourth and fifth lanes). (B) APP CTFs were normalized by housekeeping gene (β-actin) and relative band density was quantitatively analyzed ($n$=3). (C) Either wt PS1 or S353/357D PS1 was transfected into MEF PS-/- cells and APP ICD was detected by Tricin-SDS-PAGE using anti APP-C-terminal antibody. Cells were treated with 500 nM TPA that promoted the processing of APP as a positive control. (D) Membrane preparations from MEF PS-/- cells transfected with pcDNA, wt PS1 or S353/357D PS1 were incubated at 37 °C for 2 h. Control samples were kept at 4 °C. The reaction mix was then separated in pellet fraction as membrane fraction (lower panel) and supernatant fraction (first and second panels) by ultracentrifugation. These fractions were electrophoresed on polyacrylamide gradient gels or Tricine gels and immunoblotted with anti APP-C-terminal antibody. (E) APPsw/Ncad-CHO cells were incubated in Opti-MEM in the presence of 10 μM Akt inhibitor IV or 25 mM LiCl for 6 h. PS1 (S353/357) and GSK3β (S9) phosphorylation were analyzed by immunoblotting, using anti-phospho-PS1 S353/357, anti-PS1 CTF, anti-GSK3β and anti-phospho-GSK3β S9 antibodies. (F) Cell viability was analyzed by MTT assay. Both 10 μM of Akt inhibitor IV and 25 mM LiCl (GSK inhibitor) which were used in this study didn't induce cell death ($n$=10). 100 μM of Akt inhibitor was used as positive control. (G) and (H) APPsw/Ncad-CHO cells were incubated in Opti-MEM in the presence of 10 μM Akt inhibitor IV or 25 mM LiCl for 6 h. DMSO was used as a negative control. After incubation, released extracellular Aβ 40 or Aβ 42 for 1 h were analyzed by ELISA ($n$=5). (I) Extracellular Aβ 42/40 ratio was quantitatively analyzed.

in human brains. In order to rule out the post-mortem effect on the phosphorylation state of PS1 and GSK3β, we examined the levels of PS1 and GSK3β phosphorylation in mouse brains with different post-mortem intervals and demonstrated that post-mortem intervals did not influence the phosphorylation ratio of either PS1 or GSK3β up to 36 h after sacrifice (data not shown). In accordance with the previous reports, the phosphorylation ratio of GSK3β S9 was significantly decreased in AD brains compared with that in control brains (Fig. 2A, third and fourth rows, Fig. 2B), indicating the hyperactivity of GSK3β in AD brains. In contrast, PS1 phosphorylation was significantly increased in AD brains compared with that in control ones (Fig. 2A, first and second rows, Fig. 2C). These results suggest that up-regulated GSK3β activity could enhance PS1 phosphorylation in AD-affected brains.

### PS1 phosphorylation promoted IR cleavage

Since IR is one of key regulators of GSK3β activity, we analyzed the functional relationship between PS1/γ-secretase activity and IR. It is now reported that γ-secretase processes IR, a main player of insulin signaling, along with other substrates (Kasuga et al., 2007; Marambaud et al., 2002; Okamoto et al., 2001). As reported previously, ectodomain shedding of IR β-subunit by metalloproteases generates a membranous fragment—IR CTF (Fig. 3A, bottom), which is further cleaved by γ-secretase to produce the intracellular domain—IR ICD (Fig. 4A, bottom). For the analysis of IR cleavage, we co-transfected either wt PS1 or S353/357D PS1 together with IR into MEF PS-/- cells, followed by insulin treatment. In the absence of insulin, IR CTF level was slightly higher in wt PS1 cells than that in

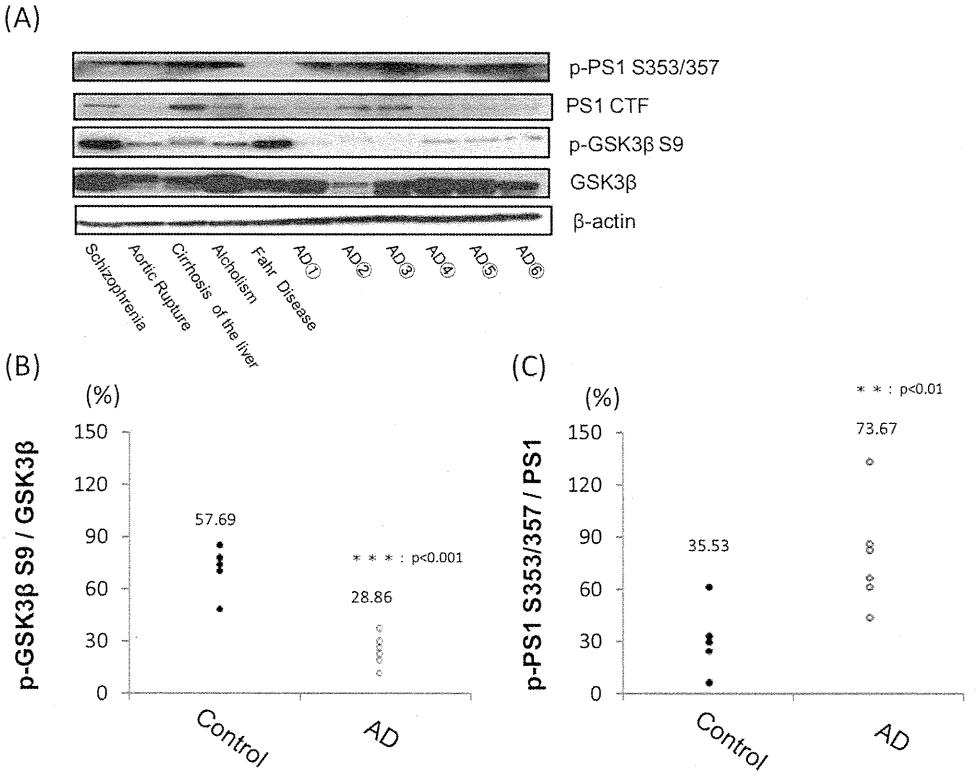


**Fig. 2.** PS1 phosphorylation is increased in AD brains. (A) The lysates of human brain samples, including AD and non-AD brains, were analyzed by immunoblotting, using anti-phospho-PS1 S353/357, anti-PS1 CTF, anti-GSK3$\beta$ and anti-phospho-GSK3$\beta$ S9 antibodies. Lording control was detected using anti-$\beta$-actin antibody (lower panel). (B, C) GSK3$\beta$ and PS1 phosphorylation ratio of each sample was quantitatively analyzed and described as a point. The number indicated on the point means average ratio.

S353/357D PS1 cells (Fig. 3B, second and third lanes). Moreover, insulin treatment led to a robust increase in the level of IR CTF in wt PS1 when compared to that in S353/357D PS1 (Fig. 3B, fourth and fifth lanes, Fig. 3C). In addition, we examined the level of IR ICD using *in vitro* $\gamma$-secretase assay and demonstrated that IR ICD level in S353/357D PS1 cells was higher than that in wt PS1 cells (Fig. 3D). These results suggested that PS1 phosphorylation enhanced the $\gamma$-secretase-mediated cleavage of IR CTF.

Since phosphorylation of PS1 reduces the PS1/N-cadherin/$\beta$-catenin interaction (Uemura et al., 2007), we asked whether the PS1 interaction with N-cadherin/$\beta$-catenin directly affects IR cleavage. To test this, MEF PS-/- cells were co-transfected with IR and $\Delta$340-350 PS1 (a deletion mutant lacking the loop domain necessary for the interaction with N-cadherin/$\beta$-catenin; Uemura et al., 2007), followed by insulin treatment. As in S353/357D PS1 transfected cells (Fig. 3E, middle lane), the level of IR CTF in $\Delta$340-350 PS1 transfected cells was significantly decreased compared to that in wt PS1 cells (Fig. 3E, left and right lanes, Fig. 3F). These findings were also confirmed in neuronal cells (Fig. 3G). Collectively, these results indicated that dissociation of PS1 from N-cadherin/$\beta$-catenin as well as phosphorylation of PS1 promotes the cleavage of IR by $\gamma$-secretase.

### IR intracellular domain up-regulates the transcription of Akt

Several lines of evidence suggest that the cleavage of membrane protein by $\gamma$-secretase, known as regulated intramembrane proteolysis (RIP), is linked to intracellular signaling events (Wolfe and Kopan, 2004; Maetzel et al., 2009). $\gamma$-secretase generates the intracellular domain (ICD) of the membranous proteins, resulting in the release of ICD from the membrane. Some ICDs translocate to the nucleus and act as transcription regulators. IR ICD also translocates to the nucleus (Kasuga et al., 2007), but its exact function remains unknown.

To examine the cellular consequence of IR-RIP, we transfected IR ICD fused with HA-Tag (Fig. 4A, bottom) into SH-SY5Y cells. Immunostaining with anti-HA antibody revealed that IR ICD was located at the nucleus as in the previous report (Fig. 4B, under panel), whereas full length IR was located at the cell membrane and in the cytoplasmic region (Fig. 4B, top panel). In order to analyze the effect of IR ICD translocation into the nucleus we transiently transfected IR ICD into native SH-SY5Y cells. 36 h after transfection, mRNA was extracted and analyzed by real-time PCR assay. In this experiment, we focused on the mRNA level of Akt, because Akt plays important roles in IR signaling. Since Akt has three isoforms—Akt 1, 2 and 3, we evaluated mRNA level of all the isoforms. mRNA

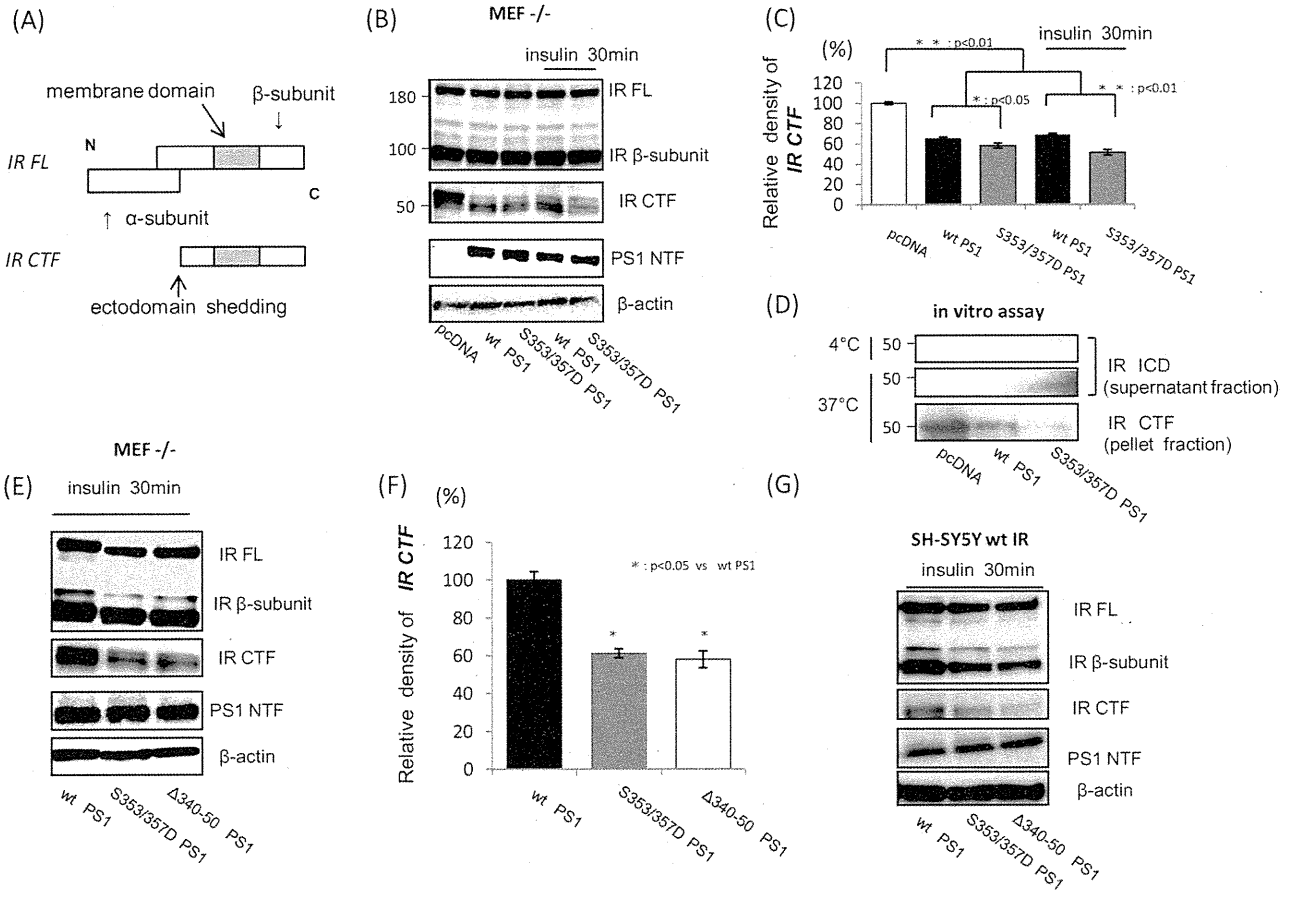


**Fig. 3.** IR cleavage is promoted by PS1 phosphorylation. (A) A schematic representation of IR CTF. IR-β-subunit is cleaved by metalloproteases at the extracellular area, producing IR CTF (bottom). (B) Either wt PS1 or S353/357D PS1 was co-transfected with IR into MEF PS-/- cells. Control cells were transfected with pcDNA (first lane). 24 h after transfection, cells were treated with 50 nM insulin for 30 min (fourth and fifth lanes). (C) IR CTF was normalized by β-actin and relative band density was quantitatively analyzed ($n$=3). (D) Membrane preparations from MEF PS-/- cells co-transfected IR with pcDNA, wt PS1 or S353/357D PS1 were incubated at 37 °C for 2 h. Control samples were kept at 4 °C. The reaction mix was then separated in pellet fraction as membrane fraction (lower panel) and supernatant fraction (first and second panels) by ultracentrifugation. These fractions were electrophoresed on polyacrylamide gradient gels and immunoblotted with anti IR-C-terminal antibody. (E) MEF PS-/- cells were transfected with wt PS1, S353/357D PS1 or Δ340-350 PS1 and after 24 h of transfection, cells were treated with 50 nM insulin for 30 min. (F) IR CTF was normalized by β-actin and relative band density was quantitatively analyzed ($n$=3). (G) SH-SY5Y wt IR cells were transfected with either wt PS1, S353/357D PS1 or Δ340-350 PS1 and then treated with 50 nM insulin for 30 min.

levels of Akt 1 and 2 were significantly increased in IR ICD transfected cells, compared with those in control cells (Fig. 4C). The protein level of total Akt was also significantly increased in IR ICD transfected cells 48 h after transfection (Fig. 4D, E), suggesting marked transactivation of Akt in IR ICD transfected cells. Moreover, under the same condition, we observed that IR ICD reduced GSK3β activity, promoted GSK3β S9 phosphorylation, as well as enhanced Akt levels (Fig. 4F, G). These results collectively indicate that IR ICD can enhance Akt transcription, followed by the reduction in GSK3β activity.

### PS1/γ-secretase-mediated IR cleavage changes the expression level of Akt

To confirm that IR-RIP regulates the transcription of Akt, we modulated IR cleavage in several ways. First, we inhibited γ-secretase activity and observed the expression level of Akt. After a 24 h DAPT treatment, the level of Akt did not change in SH-SY5Y cells which have little endogenous IR (data not shown). On the other hand, the expression level of Akt was dose-dependently decreased in SH-SY5Y wt IR cells (Fig. 5A, top row), indicating that inhibition of γ-secretase led to decrease the levels of Akt. These results were confirmed by the treatment with another γ-secretase inhibitor, L-685458 (data not shown), and by non-pharmacological inhibition (Fig. 5B, middle and right lanes), using D385A PS1, which dominant-negatively inhibits γ-secretase activity (Uemura et al., 2003).

It was reported that IR might undergo ectodomain shedding by metalloproteases such as ADAM 17 (Kasuga et al., 2007). Since protein kinase C activation enhances the metalloprotease-mediated ectodomain shedding (Ni et al., 2001), we treated SH-SY5Y wt IR cells with 500 nM TPA to enhance the ectodomain shedding. In the presence of L-685458, TPA treatment for 24 h increased the level of IR CTF, indicating that ectodomain shedding of IR was

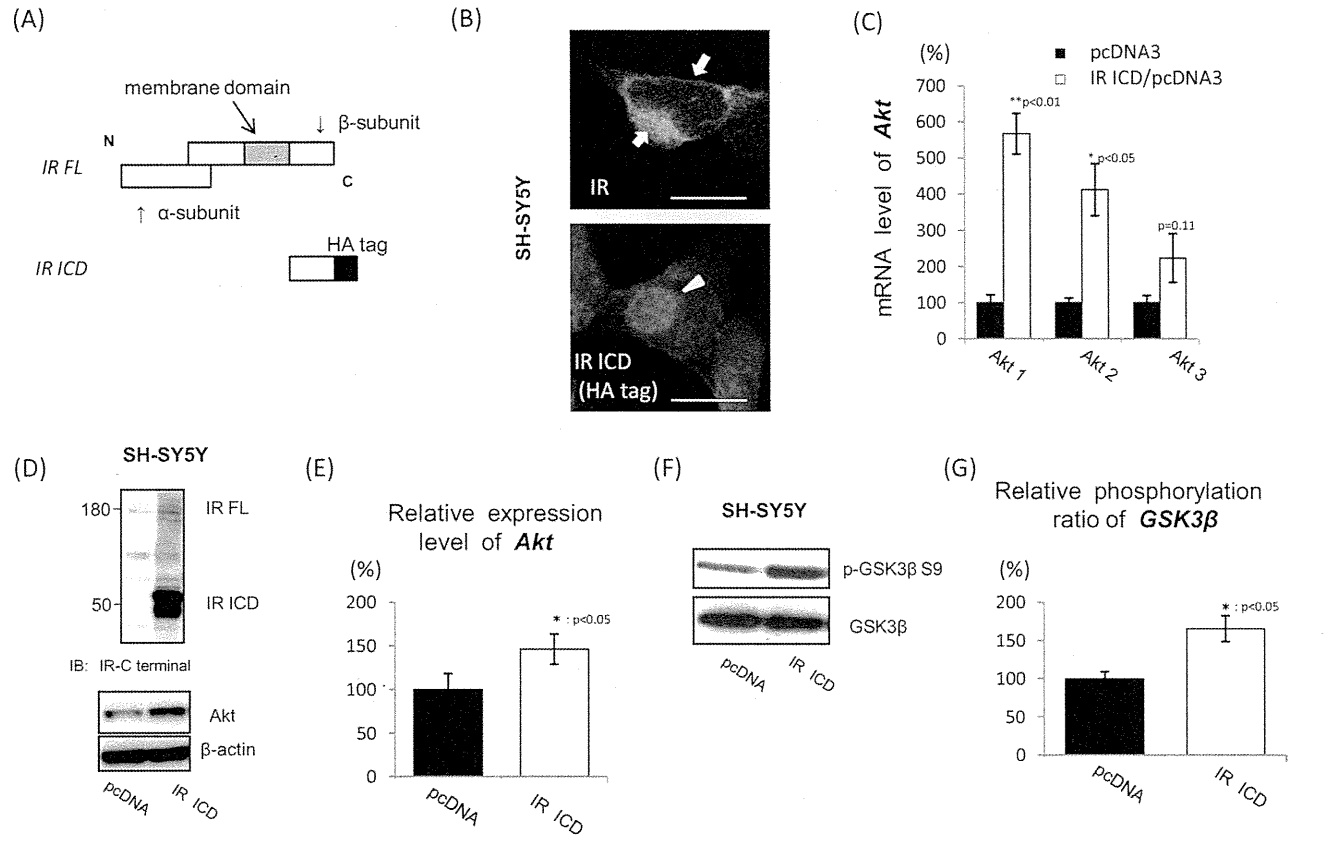


**Fig. 4.** IR ICD up-regulates the transcription of Akt. (A) A schematic representation of plasmid construction of IR ICD. The HA tag was fused to the C-terminus of IR ICD (bottom). The amino acid of transmembrane domain was indicated (top, gray area). (B) Native SH-SY5Y cells were transfected with IR ICD or full length (FL) IR. Scale bar, 20 $\mu$m. (C) SH-SY5Y cells were transfected with IR ICD. After 36 h of transfection, the mRNA levels of Akt were analyzed by real-time PCR assay. The mRNA amount of Akt was normalized by that of $\beta$-actin ($n$=4). (D) After 48 h of transfection, SH-SY5Y cells were analyzed by immunoblotting. (E) The expression level of endogenous Akt was quantitatively analyzed ($n$=3). The level of Akt was normalized by that of $\beta$-actin. (F) After 48 h of transfection of IR ICD, the level of phospho-GSK3$\beta$ S9 was analyzed by immunoblotting. (G) The relative phosphorylation ratio of GSK3$\beta$ was quantitatively analyzed ($n$=3).

promoted by TPA (Fig. 5C, third and fifth lanes). To analyze its effect on Akt levels, SH-SY5Y wt IR cells were pre-incubated with either DAPT or vehicle (DMSO) for 18 h, followed by TPA treatment with or without DAPT. Interestingly, in the absence of DAPT, the expression level of Akt was increased (Fig. 5D, fifth lane, Fig. 5E). Conversely, TPA treatment in the presence of DAPT significantly decreased the level of Akt (Fig. 5D, fourth and sixth lanes). Similarly, treatment with PKC inhibitor for 24 h in different concentrations demonstrated the dose-dependent decrease of Akt levels (data not shown). Taken together, these results indicate that $\gamma$-secretase-mediated IR cleavage generates IR ICD, which then transactivates Akt.

## DISCUSSION

Previous reports demonstrated that GSK3$\beta$ activity is up-regulated in AD brains (Bhat et al., 2004). On the other hand, conditional transgenic mice overexpressing GSK3$\beta$ in the adult brain show clear evidence of neurodegeneration (Lucas et al., 2001). Moreover, aberrantly activated GSK3$\beta$ phosphorylates Tau, which leads to NFTs (Hanger et al., 1992). This evidence clearly indicated that GSK3$\beta$ plays essential roles in the pathology of AD. Importantly, we and other groups previously reported that PS1, a causative molecule of familial AD, was also phosphorylated by GSK3$\beta$ at serine 353, 357 residues (Kirschenbaum et al., 2001; Twomey and McCarthy, 2006; Uemura et al., 2007). Since most of the familial AD-linked PS1 mutations affect APP metabolism, in the present study, we examined the effect of PS1 phosphorylation on APP cleavage by PS1/$\gamma$-secretase. Our analysis using S353/357D mutant PS1 revealed that phosphorylated PS1 significantly inhibited the cleavage of APP CTFs by $\gamma$-secretase (Fig. 1A–D). Furthermore, the ELISA results indicated that PS1 phosphorylation reduced extracellular A$\beta$ 40 levels without changing extracellular A$\beta$ 42 levels, thereby increasing the A$\beta$ 42/40 ratio (Fig. 1G–I). Similar phenomena were observed in the familial AD-linked PS1 mutations (Selkoe and Wolfe, 2007). Accumulating evidence suggests that partial loss of function in $\gamma$-secretase may lead to an increased A$\beta$ 42/40 ratio as well as to neurodegeneration (Shen and Kelleher, 2007; Wolfe, 2007). In addition, a recent report suggested that A$\beta$ 40 may inhibit A$\beta$ deposition and thus may be physiologically neuroprotective (Kim et al., 2007).

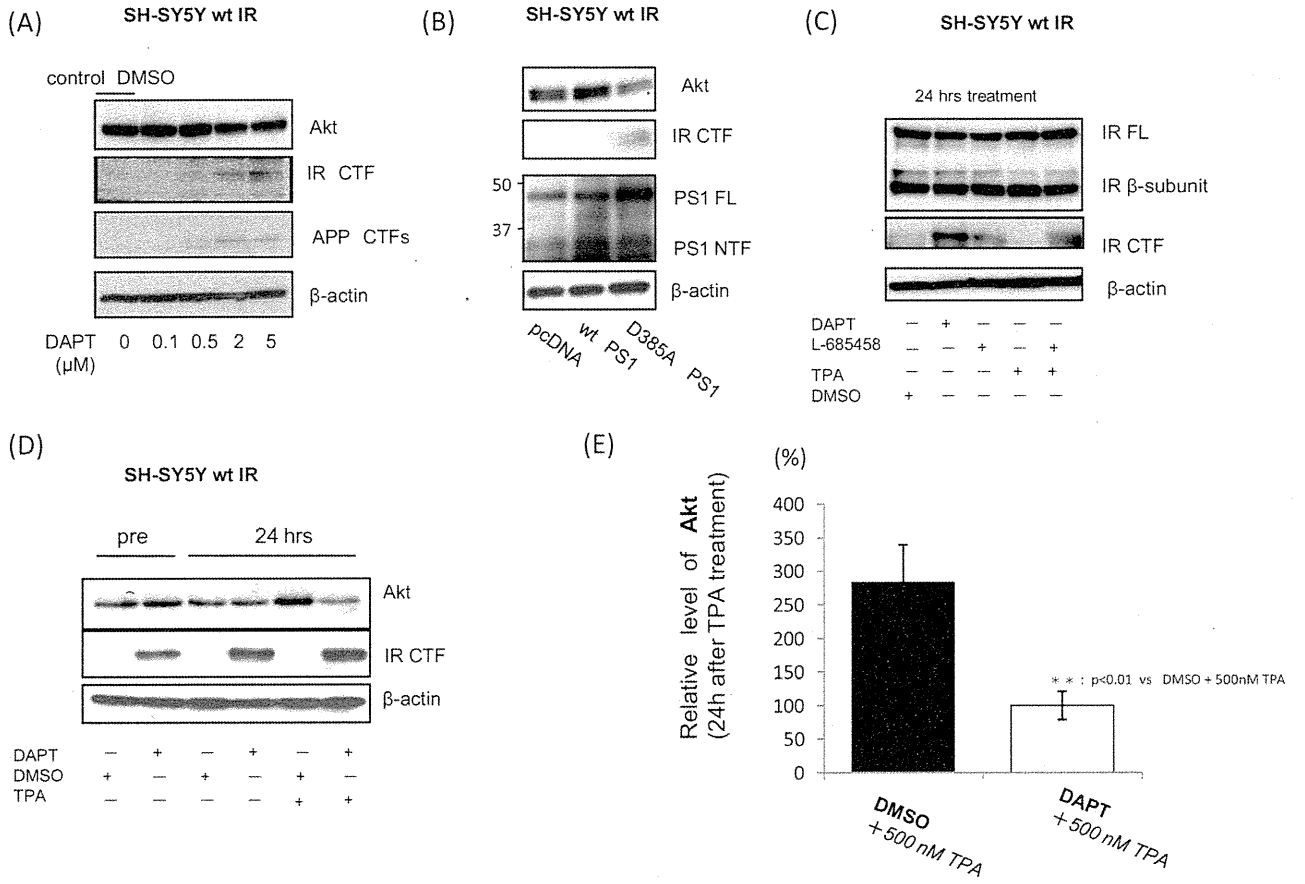


**Fig. 5.** IR cleavage changes the expression level of Akt. (A) SH-SY5Y wt IR cells were treated with DAPT for 24 h in different concentrations (0, 0.1, 0.5, 2, 5 $\mu$M). (B) SH-SY5Y wt IR cells were transiently transfected with pcDNA (as a control), wt PS1 and D385A PS1. After 48 h, the Akt level was analyzed. (C) SH-SY5Y wt IR cells were treated with 5 $\mu$M of DAPT, L-685458, 500 nM of TPA or L-685458+TPA for 24 h. Control cells were treated with DMSO. (D) After pre-incubation with either DAPT or vehicle (DMSO) for 18 h, SH-SY5Y wt IR cells were treated with 500 nM TPA in the presence of DAPT or DMSO for 24 h. (E) After TPA treatment, the relative expression level of Akt was quantitatively analyzed ($n$=4). The level of Akt was normalized by that of $\beta$-actin.

Thus, PS1 phosphorylation-mediated reduction of A$\beta$ 40 and increase of A$\beta$ 42/40 ratio can aggravate the pathology of AD (Fig. 6, left panel). So far, the significance of PS1 modification including phosphorylation has not yet been fully investigated in AD brains. Importantly, our *in vivo* study clearly showed accelerated PS1 phosphorylation in sporadic AD patient brains (Fig. 2). Considering these results, the disruption of the balance of PS1 phosphorylation may lead to neurodegeneration via aberrant GSK3$\beta$ activity.

In addition, we searched for the mechanisms inhibiting PS1 phosphorylation. In the present study, we found a novel role of $\gamma$-secretase-mediated IR cleavage as a protective safeguard from aberrant GSK3$\beta$ activity (Fig. 6, right panel). IR is widely distributed in the brain with particularly high concentrations in neurons, both in the cell bodies as well as in synapses (Werther et al., 1987; Marks et al., 1991). IR is a known substrate for $\gamma$-secretase and IR ICD translocates to the nucleus upon $\gamma$-secretase-mediated cleavage (Kasuga et al., 2007). In this report, we showed that IR ICD activates the transcription of Akt (Fig. 4), a key element in multiple biological processes including glucose metabolism, cell survival, cell growth, cell differentiation, and angiogenesis (Franke et al., 2003; Fayard et al., 2005; Song et al., 2005). Notably, we observed that PS1 phosphorylation promoted the $\gamma$-secretase-mediated cleavage of IR (Fig. 3). Thus, GSK3$\beta$ activation may promote the phosphorylation of PS1 to enhance cleavage of IR, finally activating the transcription of Akt, which is a strong inhibitor of GSK3$\beta$ activity. This phenomenon may constitute a negative feedback mechanism, which up-regulates Akt when GSK3$\beta$ is aberrantly activated. Interestingly, this is contrary to the case of the cleavage of N-cadherin, since N-cadherin cleavage is down-regulated by the phosphorylation of PS1 (Uemura et al., 2007). Thus, the phosphorylation status of PS1 may explain in part the substrate specificity in various conditions.

## CONCLUSION

We propose that GSK3$\beta$-mediated PS1 phosphorylation, acting as a link between GSK3$\beta$ activity and A$\beta$ generation, may play a pivotal role in AD pathogenesis under the influence of insulin signaling. As our study indicated that GSK3$\beta$-mediated phosphorylation of PS1 increases the A$\beta$ 42/40 ratio, modulating GSK3$\beta$ activity can be a good

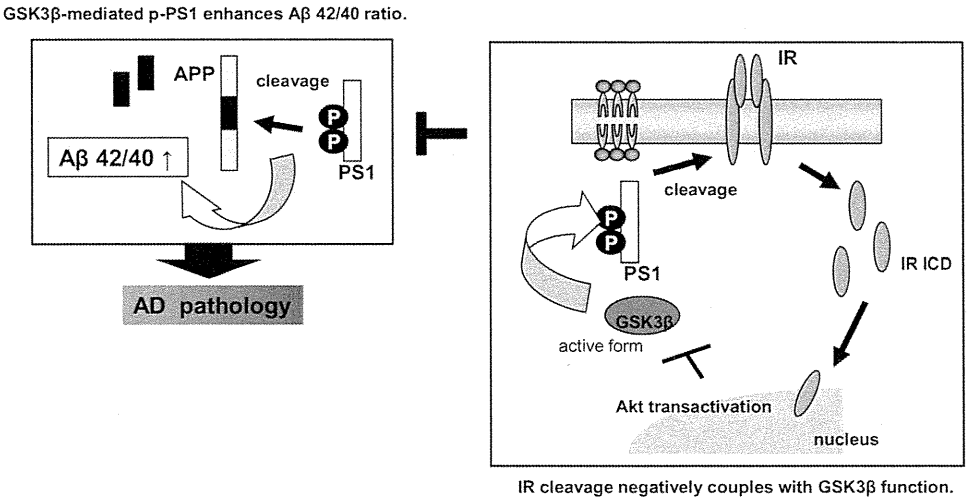


**Fig. 6.** Schematic presentation of cellular events caused by PS1 phosphorylation. GSK3$\beta$-mediated PS1 phosphorylation enhances the extracellular A$\beta$42/40 ratio and its phosphorylation is promoted in the AD brain. Therefore, PS1 phosphorylation may promote the pathology of AD (left panel). On the other hand, when GSK3$\beta$ is aberrantly activated, the phosphorylated PS1 cleaves IR, then activates the transcription of Akt, which finally inhibits GSK3$\beta$ activity (right panel). There may be some mechanisms which down-regulate PS1 phosphorylation through inhibition of GSK3$\beta$ activity and IR cleavage by $\gamma$-secretase can be one of them.

therapeutic strategy, aiming at both the inhibition of tau phosphorylation and the reduction of A$\beta$ 42/40 ratio. Thus, IR cleavage could be one of the potential regulatory mechanisms affecting GSK3$\beta$ activity as a negative feedback mechanism; disruption of IR cleavage may lead to increased GSK3$\beta$ activity, as well as A$\beta$ 42/40 ratio. Therefore, the *in vivo* regulatory mechanism of controlling PS1 function including phosphorylation should be examined in future studies.

*Acknowledgments—We greatly appreciate the gift of human Insulin Receptor (hIR) construct from Dr. T. Ikeuchi (Niigata University, Niigata, Japan), PS1/PS2 double knockout mouse embryonic fibroblast (MEF PS-/-) from Dr. B DeStrooper (Catholic University, Leuven, Belgium) and pcDNA3 with HA tag vector from Dr. R. Takahashi (Kyoto University, Kyoto, Japan). We would like to give our thanks to Dr. M. Kinoshita (Nagoya University, Nagoya, Japan) and Dr. A. Yanagida (Kyoto University, Kyoto, Japan) for technical assistance of Real-time PCR assay. We would like to give our thanks to Dr. S. Oka (Kyoto University, Kyoto, Japan), Mr. T. Kohno and Ms. N. Yamada for technical assistance of Tricine SDS-PAGE. The work was financially supported by Grant-in-Aid from the Ministry of Education, Culture, Sports, Science and Technology (20300124) and the Research Grant from Takeda Science Foundation.*

## REFERENCES

Bhat RV, Budd Haeberlein SL, Avila J (2004) Glycogen synthase kinase 3: a drug target for CNS therapies. J Neurochem 89: 1313–1317.

Braak H, Braak E (1991) Neuropathological stageing of Alzheimer-related changes. Acta Neuropathol 82:239–259.

Bradford MM (1976) A rapid and sensitive method for the quantitation of microgram quantities of protein utilizing the principle of protein-dye binding. Anal Biochem 72:248–254.

De Strooper B, Saftig P, Craessaerts K, Vanderstichele H, Guhde G, Annaert W, Von Figura K, Van Leuven F (1998) Deficiency of presenilin-1 inhibits the normal cleavage of amyloid precursor protein. Nature 391:387–390.

Ebina Y, Edery M, Ellis L, Standring D, Beaudoin J, Roth RA, Rutter WJ (1985) Expression of a functional human insulin receptor from a cloned cDNA in Chinese hamster ovary cells. Proc Natl Acad Sci U S A 82:8014–8018.

Fayard E, Tintignac LA, Baudry A, Hemmings BA (2005) Protein kinase B/Akt at a glance. J Cell Sci 118:5675–5678.

Francis R, McGrath G, Zhang J, et al. (2002) Aph-1 and pen-2 are required for Notch pathway signaling, gamma-secretase cleavage of betaAPP, and presenilin protein accumulation. Dev Cell 3:85–97.

Franke TF, Hornik CP, Segev L, Shostak GA, Sugimoto C (2003) PI3K/Akt and apoptosis: size matters. Oncogene 22:8983–8998.

Goutte C, Tsunozaki M, Hale VA, Priess JR (2002) APH-1 is a multipass membrane protein essential for the Notch signaling pathway in *Caenorhabditis elegans* embryos. Proc Natl Acad Sci U S A 99:775–779.

Grundke-Iqbal I, Iqbal K, Quinlan M, Tung YC, Zaidi MS, Wisniewski HM (1986) Microtubule-associated protein tau. A component of Alzheimer paired helical filaments. J Biol Chem 261:6084–6089.

Hanger DP, Hughes K, Woodgett JR, Brion JP, Anderton BH (1992) Glycogen synthase kinase-3 induces Alzheimer's disease-like phosphorylation of tau: generation of paired helical filament epitopes and neuronal localisation of the kinase. Neurosci Lett 147:58–62.

Kasuga K, Kaneko H, Nishizawa M, Onodera O, Ikeuchi T (2007) Generation of intracellular domain of insulin receptor tyrosine kinase by gamma-secretase. Biochem Biophys Res Commun 360: 90–96.

Kim J, Onstead L, Randle S, Price R, Smithson L, Zwizinski C, Dickson DW, Golde T, McGowan E (2007) Abeta40 inhibits amyloid deposition *in vivo*. J Neurosci 27:627–633.

Kirschenbaum F, Hsu SC, Cordell B, McCarthy JV (2001) Substitution of a glycogen synthase kinase-3beta phosphorylation site in presenilin 1 separates presenilin function from beta-catenin signaling. J Biol Chem 276:7366–7375.

Linda A, Sofia H, Gerd M, Kerstin I (2007) IGF-1-induced processing of the amyloid precursor protein family is mediated by different signaling pathways. J Biol Chem 282:10203–10209.

Lucas J, Hernández F, Gómez-Ramos P, Morán M, Hen R, Avila J (2001) Decreased nuclear beta-catenin, tau hyperphosphorylation and neurodegeneration in GSK-3beta conditional transgenic mice. EMBO J 20:27–39.

Maesako M, Uemura K, Kubota M, et al. (2010) Insulin regulates presenilin 1 localization via PI3k/Akt signaling. Neurosci Lett 483: 157–161.

Maetzel D, Denzel S, Mack B, et al. (2009) Nuclear signalling by tumour-associated antigen EpCAM. Nat Cell Biol 11:162–171.

Marambaud P, Shioi J, Serban G, et al. (2002) A presenilin-1/gamma-secretase cleavage releases the E-cadherin intracellular domain and regulates disassembly of adherens junctions. EMBO J 21: 1948–1956.

Marks JL, King MG, Baskin DG (1991) Localization of insulin and type 1 IGF receptors in rat brain by *in vitro* autoradiography and *in situ* hybridization. Adv Exp Med Biol 293:459–470.

Mirra SS, Heyman A, McKeel D, Sumi SM, Crain BJ, Brownlee LM, Vogel FS, Hughes JP, van Belle G, Berg L (1991) The Consortium to Establish a Registry for Alzheimer's disease (CERAD). Part II: standardization of the neuropathologic assessment of Alzheimer's disease. Neurology 41:479–486.

Ni CY, Murphy MP, Golde TE, Carpenter G (2001) Gamma-secretase cleavage and nuclear localization of ErbB-4 receptor tyrosine kinase. Science 294:2179–2181.

Okamoto I, Kawano Y, Murakami D, Sasayama T, Araki N, Miki T, Wong AJ, Saya H (2001) Proteolytic release of CD44 intracellular domain and its role in the CD44 signaling pathway. J Cell Biol 155:755–762.

Sastre M, Steiner H, Fuchs K, Capell A, Multhaup G, Condron MM, Teplow DB, Haass C (2001) Presenilin-dependent gamma-secretase processing of beta-amyloid precursor protein at a site corresponding to the S3 cleavage of notch. EMBO Rep 9:835–841.

Selkoe D, Wolfe MS (2007) Presenilin: running with scissors in the membrane. Cell 131:215–221.

Shen J, Kelleher RJ (2007) The presenilin hypothesis of Alzheimer's disease: evidence for a loss-of-function pathogenic mechanism. Proc Natl Acad Sci U S A 104:403–409.

Song G, Ouyang G, Bao S (2005) The activation of Akt/PKB signaling pathway and cell survival. J Cell Mol Med 9:59–71.

Steiner H, Capell A, Pesold B, Citron M, Kloetzel PM, Selkoe DJ, Romig H, Mendla K, Haass C (1998) Expression of Alzheimer's disease-associated presenilin-1 is controlled by proteolytic degradation and complex formation. J Biol Chem 273:32322–32331.

Twomey C, McCarthy JV (2006) Presenilin-1 is an unprimed glycogen synthase kinase-3beta substrate. FEBS Lett 580:4015–4020.

Uemura K, Kitagawa N, Kohno R, Kuzuya A, Kageyama T, Shibasaki H, Shimohama S (2003) Presenilin 1 mediates retinoic acid-induced differentiation of SH-SY5Y cells through facilitation of Wnt signaling. J Neurosci Res 73:166–175.

Uemura K, Kuzuya A, Shimozono Y, Aoyagi N, Ando K, Shimohama S, Kinoshita A (2007) GSK3beta activity modifies the localization and function of presenilin 1. J Biol Chem 282:15823–15832.

Uemura K, Lill CM, Banks M, et al. (2009) N-cadhrtin-based adhesion enhances Abeta release and decreases Abeta 42/40 ratio. J Neurochem 108:350–360.

Werther GA, Hogg A, Oldfield BJ, McKinley MJ, Figdor R, Allen AM, Mendelsohn FA (1987) Localization and characterization of insulin receptors in rat brain and pituitary gland using *in vitro* autoradiography and computerized densitometry. Endocrinology 121:1562–1570.

Wolfe MS (2007) When loss is gain: reduced presenilin proteolytic function leads to increased Abeta42/Abeta40. Talking point on the role of presenilin mutations in Alzheimer disease. EMBO Rep 8:136–140.

Wolfe MS, Kopan R (2004) Intramembrane proteolysis: theme and variations. Science 305:1119–1123.

Yu G, Nishimura M, Arawaka S, et al. (2000) Nicastrin modulates presenilin-mediated notch/glp-1 signal transduction and betaAPP processing. Nature 407:48–54.

*(Accepted 14 December 2010)*
*(Available online 13 January 2011)*

NEUROPATHOLOGY

*Neuropathology* 2011; **31**, 135–143 doi:10.1111/j.1440-1789.2010.01152.x

Original Article

# Gray matter lesions in Nasu-Hakola disease: A report on three autopsy cases

**Naoya Aoki,[1,6] Kuniaki Tsuchiya,[1,2] Takashi Togo,[6] Zen Kobayashi,[1,3] Hirotake Uchikado,[6] Omi Katsuse,[6] Kyoko Suzuki,[6] Hiroshige Fujishiro,[4] Tetsuaki Arai,[1] Eizo Iseki,[4] Midori Anno,[5] Kenji Kosaka,[7] Haruhiko Akiyama[1] and Yoshio Hirayasu[6]**

[1]Tokyo Institute of Psychiatry, [2]Department of Laboratory Medicine and Pathology, Tokyo Metropolitan Matsuzawa Hospital, [3]Department of Neurology and Neurological Science, Graduate School, Tokyo Medical and Dental University, [4]Department of Psychiatry, Juntendo Tokyo Koto Geriatric Medical Center, Juntendo University School of Medicine, [5]Department of Neurology, Tokyo Metropolitan Matsuzawa Hospital, Tokyo, [6]Department of Psychiatry, Yokohama City University School of Medicine and [7]Hoyu Hospital, Yokohama, Japan

**Nasu-Hakola disease is an autosomal recessively inherited disease characterized by lipomembranous polycystic osteodysplasia and sclerosing leukoencephalopathy. While white matter lesions prominent in the brain have been reported in the literature, gray matter lesions have not received particular attention. In this study, we examined three autopsy cases of Nasu-Hakola disease in order to focus specifically on gray matter lesions. The ages at onset of the three cases were 20, 23 and 29 years, and the disease durations were 29, 19 and 8 years, respectively. In addition to characteristic degeneration in the cerebral white matter, such as demyelination with conspicuous fibrillary gliosis and axonal changes, all three cases showed overt pathology in the gray matter. Neuronal loss with gliosis in the thalamus (particularly in the dorsomedial nucleus and anterior nucleus), caudate nucleus, putamen and substantia nigra was prominent in all cases, and the severity corresponded to the disease duration. The cerebral cortices were relatively preserved in all cases. One case showed neuronal loss and gliosis in the gray matter of the hippocampus, possibly due to repeated episodes of epileptic convulsions. These gray matter pathologies are considered to be responsible for some of the clinical manifestations of the disease, including extrapyramidal symptoms.**

Correspondence: Takashi Togo, MD, PhD, Department of Psychiatry, Yokohama City University School of Medicine, 3-9 Fukuura, Kanazawa-ku, Yokohama 236-0004, Japan. Email: togo.takashi@gmail.com

Received 28 January 2010; revised 8 June 2010 and accepted 6 July 2010; published online 29 September 2010.



**Key words:** gliosis, gray matter lesions, Nasu-Hakola disease, neuronal loss, polycystic lipomembranous osteodysplasia with sclerosing leukoencephalopathy (PlOSL).

## INTRODUCTION

Nasu-Hakola disease, also known as polycystic lipomembranous osteodysplasia with sclerosing leukoencephalopathy (PlOSL), was first reported at about the same time in Japan and Finland.[1-3] Subsequently, approximately 160 cases have been reported, mainly in these two countries.[4] This disease is a rare autosomal recessively inherited disease and is caused by structural defects in one of two genes encoding different subunits of the same receptor signaling complex, TREM2 and DAP12.[5,6] Both TREM2 and DAP12 form a signaling receptor complex in cells of myeloid lineage.[7,8] Dysfunction of the microglia and osteoclasts has been proposed to explain CNS and bone pathogenesis, since these cell types originate from the same myeloid lineage.[5] Its clinical features are characterized by pain in the limb bones, followed by pathological fractures and progressive dementia with prefrontal syndrome, pyramidal signs, extrapyramidal signs and apracti-aphasic symptoms. These symptoms progress steadily and are later accompanied by other symptoms, especially convulsions, eventually leading to death in middle age. The characteristic histological features are convoluted membranocystic structures observed in the systemic adipose tissues, including fatty marrow in the affected bones. In the brain, cerebral lesions are characterized by diffuse and symmetrical demyelination with conspicuous fibrillary gliosis and axonal changes in the white matter. However, to date, gray matter lesions have not received particular attention,

possibly due to the prominence of the white matter lesions. The purpose of this study was to reveal the distribution and severity of neuronal loss in gray matter lesions in three cases of Nasu-Hakola disease.

## MATERIALS AND METHODS

### Clinical history of the cases

The clinical history of the disease was verified by an independent interview with the primary caregiver. The age at onset was defined as the age at which the subject first showed obvious signs suggestive of skeletal involvement or personality change, and was estimated on the basis of family members' reports and hospital records. The three cases underwent neurological, psychological and radiological examinations.

### Neuropathological examination

Brain tissue samples were fixed post-mortem with 10% formalin and embedded in paraffin. Ten-μm-thick sections from the frontal, temporal, parietal, insular and cingulate cortex, hippocampus, amygdala, basal ganglia, midbrain, pons, medulla oblongata and cerebellum were prepared. These sections were stained with HE, KB, PAS, Holzer stain, Bodian stain, methenamine silver stain and Gallyas-Braak stain. Genetic analysis was not performed, since no frozen sections were available.

### Semi-qualitative assessment of neuronal loss

The distribution and severity of neuronal loss associated with gliosis was graded on a "–" to "+++" scale using the HE-, KB- and Holzer-stained sections: –, neither neuronal loss nor gliosis observed; +, mild neuronal loss and gliosis observed; ++, moderate neuronal loss and gliosis observed, but tissue rarefaction absent; +++, severe neuronal loss and gliosis observed with tissue rarefaction.

## RESULTS

The clinical and pathological characteristics of the three cases are summarized in Tables 1 and 2. The detailed clinical course and a part of the conventional pathological findings of Case 3 have previously been reported.[9]

### Case reports

*Case 1*

A Japanese woman developed ankle pain in her left leg at the age of 20 and roentgenograms revealed a transparent shadow in her tibia. There was no family history of related disease. Bone biopsy revealed membranocystic changes

**Table 2** Gray matter pathologies of the three cases

| | Case 1 | Case 2 | Case 3 |
|---|---|---|---|
| Brain weight (g) | 840 | 910 | 1010 |
| Neuronal loss | | | |
| Cerebral cortex | – | – | – |
| Hippocampus | +++ | – | – |
| Amygdaloid nucleus | ++ | NA | – |
| Nucleus basalis of Meynert | NA | NA | – |
| Caudate nucleus | +++ | +++ | + |
| Putamen | ++ | ++ | + |
| Globus pallidus | – | NA | – |
| Thalamus | | | |
| Dorsomedial nucleus | +++ | +++ | ++ |
| Anterior nucleus | +++ | +++ | – |
| Ventrolateral nucleus | ++ | ++ | – |
| Pulvinar nucleus | ++ | NA | NA |
| Substantia nigra | ++ | ++ | + |
| Locus coeruleus | – | – | – |
| Pontine nucleus | – | – | – |
| Dentate nucleus of cerebellum | – | – | – |
| Hypoglossal nucleus | – | – | – |
| Dorsal nucleus of vagus | – | – | – |
| Inferior olivary nucleus | – | – | – |

The degrees of neuronal loss were graded on "–" to "+++" scale using the HE, KB and Holzer-stained sections: –, neither neuronal loss nor gliosis observed; +, mild neuronal loss and gliosis observed; ++, moderate neuronal loss and gliosis observed, but tissue rarefaction absent; +++, severe neuronal loss and gliosis observed, with tissue rarefaction. NA, not available.

**Table 1** Summary of clinical features

| | Case 1 | Case 2 | Case 3 |
|---|---|---|---|
| Sex | Female | Male | Female |
| Heredity | – | + | + |
| Age at onset (years) | 20 | 23 | 29 |
| Age at death (years) | 49 | 42 | 37 |
| Disease duration (years) | 29 | 19 | 8 |
| Initial signs | Ankle pain | Personality change (talkative) | Forgetfulness, fatigue |
| Skeletal symptoms | + | + | – |
| Dementia | + | + | + |
| Pyramidal signs | + | + | + |
| Extrapyramidal signs | Brachybasia, tremor | Not described | Brachybasia, rigidity, tremor |
| Convulsion | + | + | + |

compatible with Nasu-Hakola disease. Disinhibition was observed from the age of 25, leading to personality changes such as euphoria, silly attitude, hyperactivity and shamelessness. Also, a neurological examination revealed brachybasia, tremor, dysarthria and dysmetria. Brain CT scan at that age showed mild diffuse brain atrophy, predominantly in the frontal lobes, and calcification in the bilateral basal ganglia. At the age of 34, she developed a progressive cognitive decline with impairment of episodic memory for recent events and stereotyped behavior. At the age of 40, she had difficulty with daily activities and was admitted to hospital. Thereafter, she suffered repeated convulsions. At the age of 42, she became bedridden. Her tendon reflexes in her extremities were all hyperactive, and ankle clonus appeared around that time. She developed hypokinesia and decreased response to external stimuli. These conditions persisted for several years, and she died of pneumonia and ileus at the age of 49.

*Case 2*

A Japanese man developed personality change at the age of 23. His parents were consanguineous, and his elder brother and younger sister had been diagnosed with Nasu-Hakola disease. He became talkative and often changed jobs. He repeatedly committed criminal acts and was taken into police custody for shoplifting at the age of 30. At the age of 31, he slipped and broke his left hip. Roentgenograms revealed multiple cystic lesions in many bones, and a bone biopsy revealed membranocystic changes compatible with Nasu-Hakola disease. After that, he was unable to walk, became susceptible to fractures and broke several other bones. He was admitted to the neurological ward of a hospital at the age of 32. On admission, he showed euphoria, shamelessness, memory disturbance and disorientation. He was not given a full neurological evaluation because of his multiple bone fractures. At the age of 38, he became dumb and suffered convulsions. One year later, tube feeding was started for severe dysphagia. Thereafter his condition deteriorated, and he entered an apallic state. He developed respiratory failure and finally died of pneumonia at the age of 42. His clinical diagnosis was Nasu-Hakola disease.

*Case 3*

A Japanese woman had been well until the age of 29, when she first complained of forgetfulness and fatigue. Her parents were consanguineous by the marriage of first cousins, and her younger sister had been diagnosed with typical Nasu-Hakola disease with skeletal and neuropsychiatric syndromes and membranocystic lesions in the bones. Personality change was observed from the age of 30, and she was twice arrested on the charge of theft. She developed brachybasia at the age of 32. She was admitted to the neurological ward of a hospital at the age of 35. On admission, she showed euphoria, apathy, memory disturbance and disorientation. Neurological examination revealed brachybasia, dysarthria, rigidity, tremor, hyperactive deep tendon reflex, bilateral Babinski's sign, ankle clonus and urinary incontinence. She soon developed convulsions. Her syndromes progressively worsened, with marked euphoria, disturbance of attention, aspontaneity, perseveration, amnestic syndrome, disorientation and dementia. She died of ileus at the age of 37. During her clinical course, no skeletal involvement or X-ray abnormality in the bones were revealed. She was pathologically diagnosed as having Nasu-Hakola disease based on findings such as membranocystic lesions in the adipose tissues and leukodystrophy in the brain.

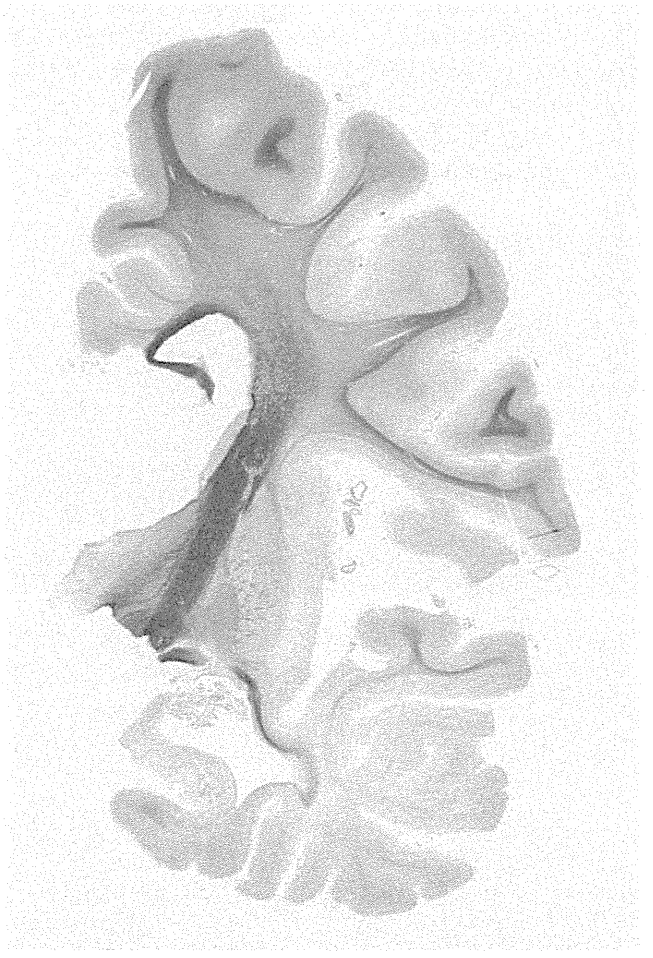

**Fig. 1** Coronal section at the level of the globus pallidus. The caudate head is flattened and the thalamus is markedly atrophic. The lateral ventricles are extremely enlarged. Volume loss and myelin pallor were seen predominantly in the temporal lobe. KB stain. (Case 1)